NEUROSCIENCE

Ciliary protein Kif7 regulates Gli and Ezh2 for initiating the neuronal differentiation of enteric neural crest cells during development

Frank Pui-Ling Lai[1†], Zhixin Li[1†], Tingwen Zhou[1†], Adrian On Wah Leung[1], Sin-Ting Lau[1], Kathy Nga-Chu Lui[1], William Yu-Ming Wong[1], Pak-Chung Sham[2], Chi-Chung Hui[3], Elly Sau-Wai Ngan[1]*

Gastrointestinal motility disorders occur frequently in patients with ciliopathy, but the underlying genetic link is unclear. The ciliary protein Kif7 can positively or negatively regulate Hedgehog signaling in different cellular contexts. Mice with neural crest cell (NCC)–specific *Kif7* deficiency show a marked reduction of enteric NOS$^+$ inhibitory neurons. Malformation of enteric nervous system (ENS) causes growth retardation and gut motility defect in mice. Mechanistically, *Kif7* inhibits Gli2 in enteric NCCs (ENCCs), where Gli2 positively regulates the expression of Ezh2 by inhibiting the *miR124*-mediated suppression. In developing ENCCs, Ezh2 is a master regulator of 102 core genes underlying ENCC differentiation. Deletion of *Gli2* or inhibition of Ezh2 favors the neurogenic lineage differentiation of mouse and human ENCCs and rescues the ENS defects of *Kif7* mutants. In summary, Hedgehog signal, via Kif7-Gli-Ezh2, controls the timely expressions of the core genes to mediate the differentiation of ENCCs.

INTRODUCTION

Chronic constipation and gastrointestinal dysmotility are common problems that affect many pediatric and adult patients. In these patients, enteric motility disorders are mainly due to abnormalities in the smooth muscle layer of the bowel or the enteric nervous system (ENS), albeit some of these disorders are associated with inflammation. Intriguingly, chronic constipation occurs frequently in pediatric patients with ciliopathies or other congenital diseases. The physiopathological mechanism underlying chronic constipation in these patients is complex and involves at least two different intestinal histopathological aspects. Some patients present with Hirschsprung (HSCR) disease with a complete absence of enteric ganglia in the distal part of the intestine, whereas in other patients the disorder appears to be the result of chronic intestinal pseudo-obstruction (CIPO) or enteric dysmotility (ED), with persistence of ganglion cells in the bowel and without a mechanical occluding lesion (*1*). With regard to understanding the disease etiology, HSCR is best characterized, whereas little progress has been made in determining the causes of non-HSCR conditions.

The ENS is primarily derived from enteric neural crest cells (ENCCs). Formation of a functional ENS requires precise coordination between neurogenesis and gliogenesis, as well as proliferation and migration of ENCCs (*2*, *3*). Disruption of any of these processes may result in incomplete colonization of the gut by ENCCs (intestinal aganglionosis), as seen in HSCR disease or intestinal hypoganglionosis that leads to functional defects such as CIPO/ED. In addition, hyperganglionosis (increased density of submucosal ganglia) and ectopic ganglia are also observed in various clinical contexts; these abnormalities may be observed in the transitional zone between aganglionic and ganglionic gut in patients with HSCR, proximal to various obstructive lesions, and in patients with CIPO, suggesting that the proper density and organization of the enteric ganglia are prerequisites for a functional ENS.

Hedgehog signaling is implicated at almost every step of gut organogenesis and ENS development (*4*–*8*). Hedgehog pathway activity is determined by the combined actions of three Gli transcription factors, Gli1, Gli2, and Gli3. Gli2 contributes to most of the primary Gli activator (Gli^A) activity. Full-length form of Gli3 (Gli3^A) also serves as an activator, whereas the truncated form of Gli3 functions largely as a repressor (Gli^R). Gli1 is a direct target of Hedgehog signaling and acts secondarily to reinforce Gli^A function. In addition, mammalian Hedgehog signal transduction relies on the integrity of the primary cilium (*9*). The kinesin motor protein Kif7 is one of the key molecules for Hedgehog signaling; it may promote ciliary trafficking and accumulation of Gli at the cilium tip and induce the microtubule-dependent translocation of Gli to the nucleus (*10*) and/or organize and stabilize the cilia tip (*11*). In humans, *KIF7* has been causally associated with various ciliopathies including the acrocallosal, Bardet-Biedl, Pallister-Hall, and Joubert syndromes (*12*–*14*). A portion of patients who suffer from these syndromes also present with HSCR or other gut motility disorders (*15*–*17*), suggesting that Kif7 may represent a causal link between ciliary dysfunction and disorders in gastrointestinal motility.

Enhancer of zeste homolog 2 (Ezh2) is a prominent histone-modifying protein; it forms a polycomb repression complex 2 (PRC2) complex with Suz12 and Eed to repress gene expression by promoting histone methylation. It also binds directly to the regulatory regions of its target genes to induce their expressions (*18*–*20*). EZH2 has been implicated in many cellular processes and diseases. Silencing function of EZH2 plays a central role in melanoma formation by suppressing ciliary genes, and that promotes primary cilium disassembly (*21*). Ezh2 also controls the choice between neuronal and astrocyte differentiation (*22*) and interacts with Gli3 to repress Hedgehog activation during limb formation (*23*). Here, we establish that Kif7 serves as a negative regulator of the Hedgehog pathway, preventing the aberrant activation of Hedgehog signaling and thereby

[1]Department of Surgery, Li Ka Shing Faculty of Medicine, University of Hong Kong, Pokfulam, Hong Kong. [2]Department of Psychiatry, Li Ka Shing Faculty of Medicine, University of Hong Kong, Pokfulam, Hong Kong. [3]Program in Developmental and Stem Cell Biology, The Hospital for Sick Children, and Department of Molecular Genetics, University of Toronto, Toronto, Ontario M5G1L7, Canada.
†These authors contributed equally to this work.
*Corresponding author. Email: engan@hku.hk

timely regulating the expression level of Ezh2 in ENS progenitors to control the differentiation of the ENCCs.

RESULTS

Kif7 mutants exhibit growth retardation and gut motility disorders

Kif7 is a key regulator in the Hedgehog pathway and is causally associated with various ciliopathies. *Kif7* null mice recapitulate human ciliopathy–related phenotypes such as exencephaly and polydactyly, but these mice die at birth (*10*, *24*). Therefore, we conditionally knocked out *Kif7* in NCCs (*Kif7 cKO*) to generate a model of ciliopathy-associated gut motility disorder, a common but complex clinical condition, as a means of revealing the general mechanism underlying gut motility disorders in patients with ciliopathy.

We used *Wnt1-Cre* to conditionally delete the *Kif7* (*Kif7*$^{f/f}$) locus in NCC lineages, including the ENS. The expected ratio of *Kif7* cKO (*Wnt1-Cre*;*Kif7*$^{f/f}$) was obtained at weaning [postnatal day 21 (P21)], but the body weight and survival of the mutants were obviously reduced relative to those of their control littermates (Fig. 1, A and B). Approximately 20% of the mutants died within the first 5 weeks after birth. In most of the moribund mutants, the gastrointestinal tract was completely filled with black stool (Fig. 1C, middle), implying that gut dysfunction likely accounts for the increased lethality of *Kif7* cKO. The remaining animals also showed a moderate gut phenotype in which some segments of the large bowel were abnormally contracted and dilated, with accumulation of small fecal pellets (Fig. 1C, bottom). The abnormal accumulation of small fecal pellets was mainly found in the colons of *Kif7* cKO mice, suggesting that colonic transit in these mice may be affected. We therefore assayed the motility of colons dissected from 3- to 4-week-old control and *Kif7* cKO mice. Colonic contractions were analyzed by monitoring the propagation of colonic migrating motor complexes (CMMCs) in the colon preparations, as previously described (*25*). Oro-anal propagating CMMCs were consistently found in colon preparations from control mice, whereas *Kif7* cKO colon preparations repeatedly failed to generate peristalsis, and only subtle and irregular contractile activity was detected. The overall speed of stool movement was significantly lower in *Kif7* cKO colons than in controls (Fig. 1D and movie S1), suggesting that colonic movement is severely affected in *Kif7* cKO mice.

Loss of Kif7 interrupts the formation of nNOS$^+$ inhibitory neurons and the submucosal plexus

The profound gut motility defect observed in *Kif7* cKO mutants was not attributable to the absence of nerve cells from the colon. Myenteric and submucosal plexuses were disorganized and not properly formed in the mutants (Fig. 2). Myenteric neurons (HuD$^+$) and Tuj1$^+$ interganglionic axons were found in the colons of 3- to 4-week-old control and mutant mice. No obvious difference in the number of glial fibrillary acidic protein–positive (GFAP) glia in control and mutant colons was observed. Nonetheless, neurons (HuD$^+$) and glia (GFAP$^+$) were unevenly distributed along the bowel and were improperly organized within the myenteric ganglia of *Kif7* cKO mice. Giant ganglia were observed in some regions of the distal colon and distal small intestine (Fig. 2B), and neurons were outnumbered by glia in some enteric ganglia of the bowels of *Kif7* cKO mice (fig. S1). The sizes of the myenteric plexuses in control and *Kif7* cKO colons were

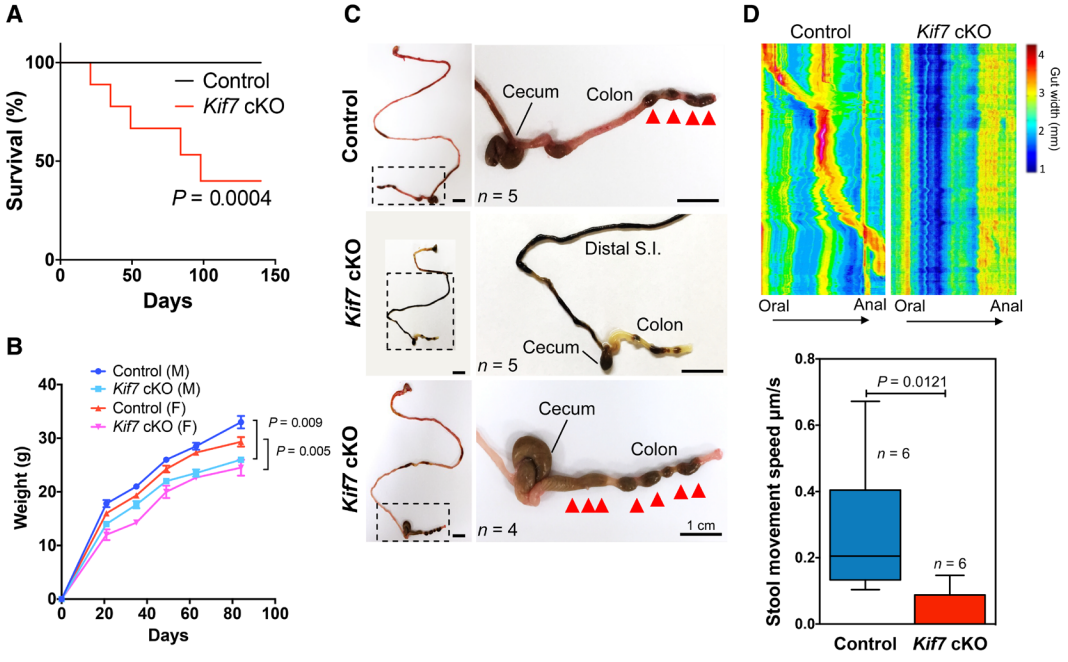

Fig. 1. *Kif7* mutants exhibit growth retardation and gut motility defects. (**A**) Kaplan-Meier graph of the survival of control (*Kif7*$^{f/f}$) and *Kif7* cKO (*Wnt1-Cre*;*Kif7*$^{f/f}$) mice. (**B**) The growth curves were generated by measuring the weights of male and female control and *Kif7* cKO mice from P0 to P84 (three to eight mice in each group). (**C**) Photomicrographs of whole gastrointestinal tract preparations from P21 control and *Kif7* cKO mice. The arrowheads indicate individual fecal pellets in colon preparations from control and mutant animals. (**D**) Video recordings of the contraction patterns of control and *Kif7* cKO colons were analyzed using spatiotemporal maps; the overall stool movement speed in control and *Kif7* cKO colons is shown in the bar chart. Error bars indicate ± SEM of the values obtained for six samples. Distal S.I., distal small intestine. Scale bars, 1 cm.

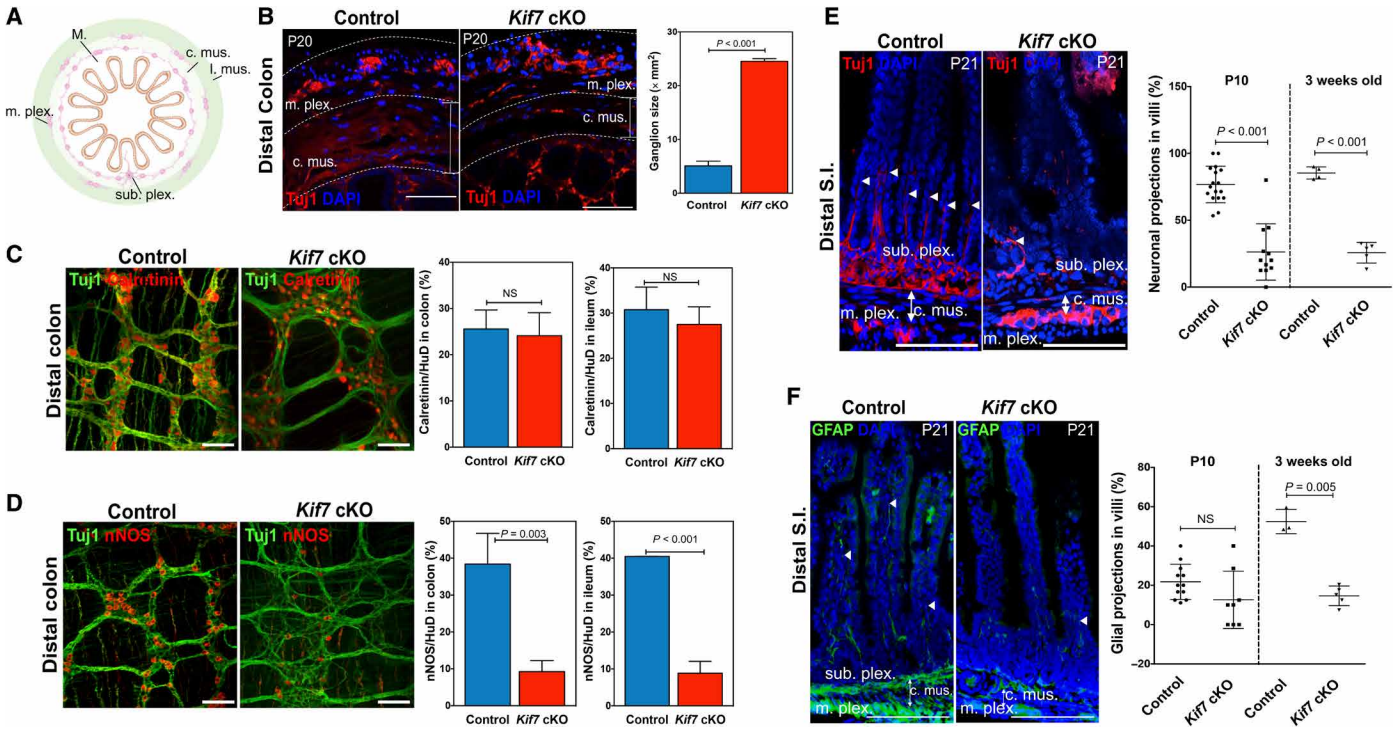

Fig. 2. Ablation of *Kif7* interferes with the formation of myenteric and submucosal neurons and gut colonization. (**A**) Schematic of the organization of the intestine. (**B**) Transverse sections of P20 control and *Kif7* cKO colons. Myenteric ganglia were marked using anti-Tuj1 antibody; the size of the ganglia was measured and is shown in the bar chart. (**C**) The excitatory and inhibitory neurons in the myenteric plexuses of the distal colons of control and *Kif7* cKO mutants (P21) were detected using antibodies against (C) calretinin and (**D**) nNOS, respectively. The numbers of excitatory (calretinin$^+$) and inhibitory (nNOS$^+$) neurons as a percentage of the total number of neurons (HuD$^+$) were determined and are shown in the bar charts. Immunohistochemistry analyses for the detection of submucosal plexuses and (**E**) neuronal (Tuj1$^+$) and (**F**) glial (GFAP $^+$) processes in villi with the transverse sections of the distal small intestine of control and *Kif7* cKO (P21). The neuronal and glial processes are marked with arrowheads. The percentages of villi with neuronal and glial processes were measured at P10 and P21 and are shown in the scatterplots. The error bars indicate ± SEM of the values obtained from at least six samples. c. mus., circular muscle; l. mus., longitudinal muscle; m. plex., myenteric plexus; sub. plex., submucosal plexus.; M., mucosa. Scale bars, 100 μm. DAPI, 4′,6-diamidino-2-phenylindole. NS, not significant.

measured in cross sections stained for the pan-neuronal marker Tuj1. Consistently, the average ganglion size was significantly larger in *Kif7* cKO mutants than in control mice (Fig. 2B), and this was accompanied by reduced thickness of the circular muscle. With respect to the two major nonoverlapping subtypes of neurons, the number of excitatory neurons (calretinin$^+$) in control and mutant mice was quite comparable (Fig. 2C), but the number of late-born inhibitory [neuronal nitric oxide synthase–positive (nNOS$^+$)] neurons was markedly reduced in the distal colon and distal small intestine of *Kif7* cKO mice (Fig. 2D).

Development of the submucosal plexus begins during the late embryonic stage and continues for a few weeks after birth (*26*). In control mice, neuronal processes derived from the submucosal plexuses could be found in the villi of the distal small intestine as early as P10, and glial projections were observed to be emerging at this stage. The number of glial projections to villi increased gradually during the first three postnatal weeks. Loss of *Kif7* adversely affected the development of submucosal plexuses. A marked reduction in the numbers of neuronal and glial cells was observed in the submucosal layer of *Kif7* cKO mutants, and only very limited numbers of villi were invaded by neuronal (Fig. 2E) and glial (Fig. 2F) projections at P10 and P21 in these mice.

Kif7 cKO ENCCs show loss of directionality

In addition to the aberrant neuronal differentiation, a delay in gut colonization (Fig. 3A) by ENCCs were observed in embryonic day 12.5 (E12.5) *Kif7* cKO (*Wnt1-Cre*;*Kif7*$^{f/f}$;*Rosa26*^{YFP}) mutants. Time-lapse imaging of the in vivo migratory behavior of ENCCs within the hindgut further revealed that the leading cells in *Kif7* cKO mutants migrate erratically and show no obvious migratory pattern (Fig. 3B and movie S2). The speed of migration of individual cells in the guts of control and mutant mice was highly comparable (Fig. 3C). However, the overall persistence and the net migration were significantly reduced in *Kif7* cKO mice because of the erratic migratory pattern of the mutant cells (Fig. 3C). The erratic migration pattern of *Kif7* cKO ENCCs may account for the uneven and incomplete colonization of the midgut and in a concomitant decrease in ENCC density in the colonized region of the hindgut, as shown in Fig. 3D.

Kif7 is crucial for the generation of neuronal precursors and enteric neurons

The generation of mature neurons and glia from NCCs during ENS development is a multistep process. Vagal NCCs become bipotent once they enter the gut, and these bipotent ENS progenitors subsequently commit to either neuronal (neuronal precursor) or glial

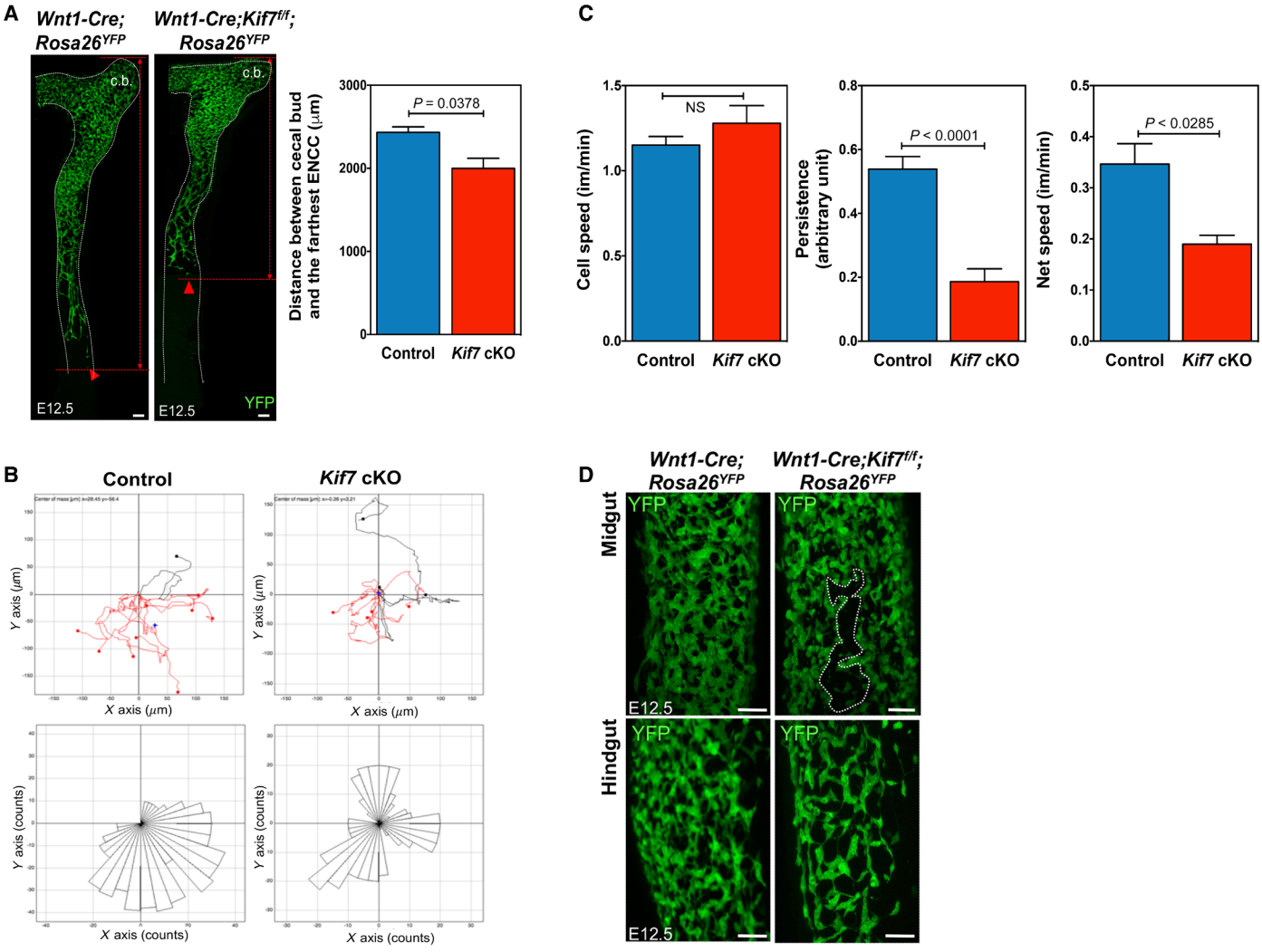

Fig. 3. Defects in migration and gut colonization in Kif7 mutants. (**A**) Whole-mount images of E12.5 control (*Wnt1-Cre;Rosa26*^{YFP}) and *Kif7* mutant (*Wnt1-Cre;Kif7*$^{f/f}$*;Rosa26*^{YFP}) guts; ENCCs were YFP$^+$. The distance from the cecal bud (c.b.) to the furthest ENCC (as indicated by the arrows) in control and mutant guts was measured and is shown in the bar chart. (**B**) Top: Chemotaxis plot from time-lapse movies of the hindgut of E12.5 control and *Kif7* cKO. Ten and seven tracks were counted in control and *Kif7* cKO samples, respectively. The migratory tracks of cells moving upward and downward relative to the center of mass (blue cross) are shown in red and black, respectively. Bottom: Polar histograms representing the trajectories of the most caudal cell at 5-min intervals in three explants of E12.5 hindgut. (**C**) Cell speed of ENCCs at the migratory wave front, persistence, and net speed are presented in the bar charts. (**D**) Whole-mount immunostaining with GFP antibody was performed on E12.5 control and *Kif7* cKO guts. The uncolonized region is marked by a dashed line.

(glial precursor) lineages and subsequently give rise to HuC/D$^+$ neuronal (NP) or B-Fabp$^+$ glial (GP) progenitors, respectively. In each developmental window, the ENS progenitors (Ret$^+$/Sox10$^+$), neuronal (Tuj1$^+$)/glial (Sox10$^+$/B-Fabp$^+$) precursors, and their progenies may or may not coexist in various proportions (Fig. 4A). The timely control of the formation of NP and GP is crucial for the proper development of a functional ENS with a full diversity of neurons and glia as well as for gut colonization (*27*).

Substantial reductions in the number of late-born inhibitory and submucosal neurons were observed in *Kif7* cKO mice. We reasoned that the neuronal precursor (Tuj1$^+$) and/or progenitor (Ret$^+$/Sox10$^+$) pools for the myenteric and submucosal plexuses are deficient in the *Kif7* cKO mice. Therefore, we quantified the ENS progenitors of the myenteric and submucosal plexuses in the embryonic gut at E11.5 and E18.5, respectively. Embryonic guts were collected from E11.5 *Wnt1-Cre;Rosa26*^{YFP} and *Wnt1-Cre;Kif7*$^{f/f}$*;Rosa26*^{YFP} embryos in which all ENCCs were marked by yellow fluorescent protein (YFP). At E11.5, most ENCCs were either bipotent progenitors (BPs) (YFP$^+$/Tuj1$^-$) or neuronal precursors (YFP$^+$/Tuj1$^+$). We found that approximately 50 to 60% of YFP$^+$ ENCCs have already been committed to the neuronal lineage and acquired neuronal identity (Tuj1$^+$) in E11.5 control intestine, whereas only ~25% of YFP$^+$ cells in the mutant intestines at this stage were committed to the neuronal lineage. Similarly, a significant reduction in the percentage of Tuj1$^+$/YFP$^+$ cells was observed in the stomachs of *Kif7* cKO mice, while no obvious change in the total number of ENCCs (YFP$^+$) was detected at this stage in *Kif7* cKO animals (Fig. 4B). As a consequence of the diminished neuronal precursor (YFP$^+$Tuj1$^+$) pool observed at E11.5, a significant reduction in neuronal number (HuC/D$^+$) was found in the guts of E13.5 embryos; this resulted in a reduced neuron-to-glia

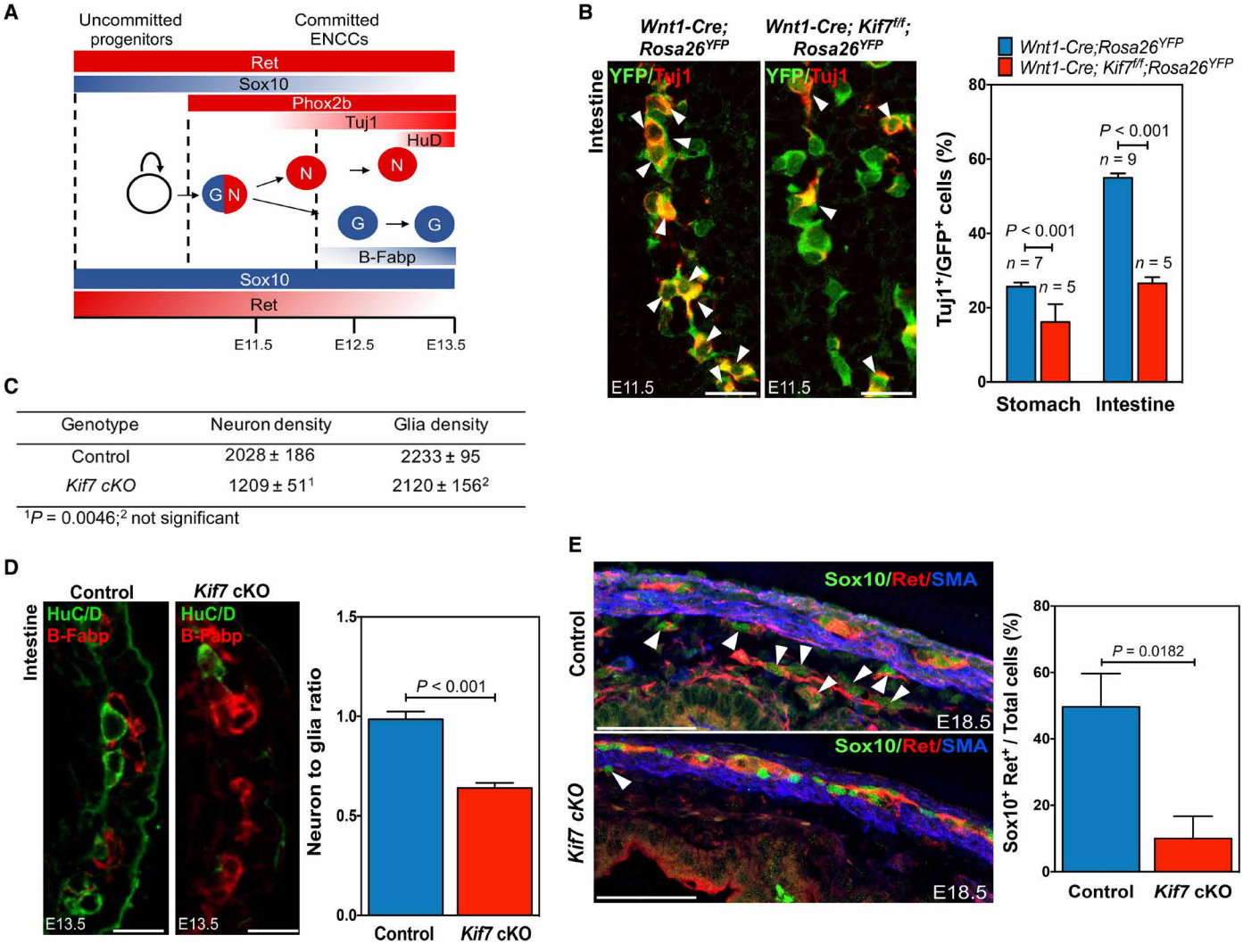

Fig. 4. Reduction in the number of neuronal precursors and enteric neurons in *Kif7* cKO mice. (**A**) Schematic diagram illustrating the subtypes of ENCCs and their expression markers during ENS development. (**B**) Immunohistochemistry showed the neuronal precursors (NP_{early}: Tuj1$^+$ YFP$^+$) (filled arrowheads) in the transverse sections of E11.5 control (*Wnt1-Cre;Rosa26*^{YFP}) and *Kif7* mutant (*Wnt1-Cre;Kif7*$^{f/f}$*;Rosa26*^{YFP}) guts. *n* = number of embryos analyzed. Scale bars, 50 μm. The number of neuronal precursors in the control and mutants as a percentage of the total number of YFP$^+$ ENCCs was measured and is shown in the bar chart. (**C**) Table shows the densities of neuronal and glial (cell number/mm^2) progenitors in E13.5 control and *Kif7* cKO hindguts, as revealed by immunohistochemistry with neuronal (HuC/D) and glial (B-Fabp) markers. (**D**) Neuron (HuC/D$^+$)–to–glia (B-Fabp$^+$) ratios in E13.5 control and *Kif7* cKO guts were measured and are shown in the bar chart (*n* = 6). Scale bars, 25 μm. (**E**) The progenitors (Ret$^+$ Sox10$^+$) of the submucosal plexuses and muscle layer (SMA$^+$) were detected in E18.5 guts using immunofluorescence. The number of progenitor cells (arrowheads) was measured as a percentage of the total number of ENCC derivatives—progenitors (Ret$^+$ Sox10$^+$), neurons (Ret$^+$ Sox10$^-$), and glia (Ret$^-$ Sox10$^+$) in control and *Kif7* cKO colons—and is shown in the bar chart. The error bars indicate ± SEM for 5 to 12 transverse sections from six embryos. Scale bars, 50 μm.

ratio, as shown in Fig. 4 (C and D). This might suggest that the observed reduction of inhibitory neurons in *Kif7* cKO mice is the result of a defect in neuronal lineage differentiation rather than an insufficiency of ENCCs. The number of glial cells (B-Fabp$^+$) was comparable in control and *Kif7* cKO mice at E13.5 (Fig. 4C). Reduced number of neuronal cells (HuC/D) led to a significant drop in the neuron-to-glia ratio in the developing guts of *Kif7* cKO mice (Fig. 4D). These data collectively suggest that Kif7 is crucial for the formation of neuronal precursors in the gut.

The ENS progenitors reach the submucosal layer at a later stage of development and participate in the formation of the submucosal plexuses. At E18.5, only very few ENS progenitors (Sox10$^+$/Ret$^+$) were found in the submucosal layer of *Kif7* cKO colons, while significantly more Sox10$^+$/Ret$^+$ cells were found in control mice (Fig. 4E). Comparable numbers of ENCCs were consistently detected in E13.5 control and *Kif7* cKO guts as measured by flow cytometry (fig. S2). Therefore, the reduced number of ENS progenitors in the submucosal layer is not likely to be due to an insufficient number of ENCCs. Instead, it might be the consequence of a migration defect of *Kif7* cKO ENCCs such that the ENS progenitors were unable to reach the submucosal layer to support the formation of submucosal plexuses.

Down-regulation of miR124 disrupts the neuronal lineage differentiation of Kif7 KO ENCCs

Our functional data suggest that NCC-specific ablation of *Kif7* adversely affects ENS development by reducing the number of Tuj1$^+$

neuronal precursors and disrupting ENCC migration. To further investigate the molecular events that occurred upon the deletion of *Kif7* in ENCCs, we examined the transcriptomes of control and *Kif7* KO ENCCs. ENCCs were isolated from E11.5 $Kif7^{f/f}$ embryonic guts and infected with adenoviruses expressing green fluorescent protein (GFP) or Cre recombinase to generate control and $Kif7^{-/-}$ ENCCs, as previously described (Fig. 5A) (*4*). Activation of the Hedgehog pathway was observed as revealed by quantitative reverse transcription polymerase chain reaction (RT-qPCR), which showed that *Gli1*, *Gli2*, and *Ptch1* transcripts were significantly up-regulated (Fig. 5B). By Western blotting, Gli2 protein was found to be consistently up-regulated in $Kif7^{-/-}$ ENCCs, and the amount of transcriptional repressor, as reflected by the ratio of processed ($Gli3^{R}$) to full-length Gli3 ($Gli3^{A}$), was decreased; no obvious change in Gli1 levels was observed (Fig. 5C). From the bulk RNA sequencing (RNA-seq) data, we identified 969 differentially expressed genes (DEGs) in $Kif7^{-/-}$ ENCCs representing 374 up-regulated and 595 down-regulated genes in comparison with the control ENCCs (Ad-GFP) ($\log_2$ fold change ≥ 1.5; adjusted $P < 0.05$). A robust up-regulation of numerous Hedgehog target genes (*Gli1*, *Gli2*, *Hes1*, *Nkx3.1*, and *Irx3*) was observed, accompanied by down-regulation of a panel of genes implicated in ENS development and neurogenesis (*Ret*, *Phox2b*, *Sox10*, *AsclI*, etc.) (Fig. 5D). Analysis of the top 10 Gene Ontology (GO) terms revealed that down-regulated genes in $Kif7^{-/-}$ ENCCs were primarily enriched in terms related to autonomic nervous system development. The corresponding expression patterns of the most relevant genes are shown in the heatmap in Fig. 5E. In particular, genes specifically expressed in neuronal lineages (*Phox2a*, *Phox2b*,

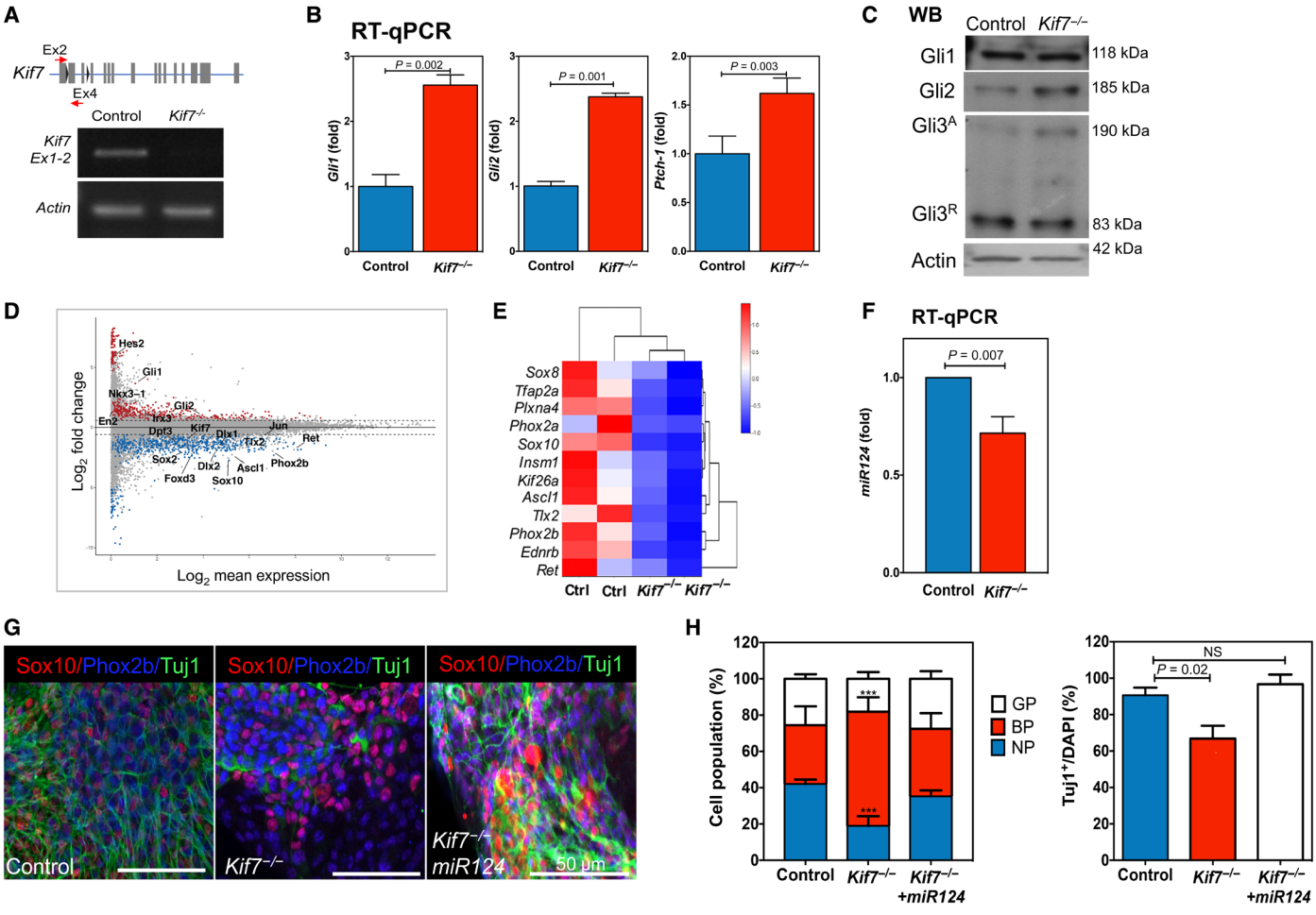

Fig. 5. *miR124* enhances the neuronal differentiation capacity of $Kif7^{-/-}$ ENCCs. (**A**) ENCCs were isolated from E11.5 $Kif7^{f/f}$ embryonic guts, which have *loxP* sites flanking exons 2 to 4 of the *Kif7* gene. $Kif7^{f/f}$ ENCCs were then infected with the control (Ad-GFP) or Cre-encoding (Ad-GFP-Cre) adenovirus. PCR product was generated with primers spanning exons 1 to 2 of *Kif7* to distinguish the wild-type and deleted *Kif7* transcripts. (**B**) The expressions of the Hh target genes in control and $Kif7^{-/-}$ ENCCs were analyzed by RT-qPCR. (**C**) Western blot analyses showing Gli expression in control and $Kif7^{-/-}$ ENCCs. Actin was used as a loading control. (**D**) Bulk RNA-seq was performed with control (Ad-GFP) and $Kif7^{-/-}$ (Ad-GFP-Cre) ENCCs. The plot shows the relationship between average gene expression ($\log_2$ mean expression) and $\log_2$ fold change (FC) in the control compared with $Kif7^{-/-}$ ENCCs. A selection of Hh target genes and genes involved in ENS development and neurogenesis is highlighted in black. Blue, $\log_2$ FC ≤ -1.5, $P < 0.05$; gray, $\log_2$ FC > -1.5 or $\log_2$ FC < 1.5, $P > 0.05$; red, $\log_2$ FC ≥ 1.5, $P < 0.05$. (**E**) Gene Ontology (GO) terms associated with autonomic nervous system development genes up-regulated in control (red) and down-regulated in $Kif7^{-/-}$ (blue) are shown in the heatmap. (**F**) Bar chart shows the relative expression level of *miR124* in control and $Kif7^{-/-}$ ENCCs as revealed by RT-qPCR. (**G**) In vitro differentiation assay, the control, and $Kif7^{-/-}$ ENCCs. $Kif7^{-/-}$ ENCCs transfected with *miR124* were cultured with GDNF for 5 days. The differentiation capacity of ENCCs was monitored on the basis of the expressions of Tuj1, Sox10, and Phox2b, as revealed by immunocytochemistry. (**H**) Charts show the quantitative analyses. The error bars indicate ± SEM of the values obtained from three independent experiments.

Ret, *Ascl1*, etc.) were found to be significantly down-regulated in *Kif7*$^{-/-}$ ENCCs. We then examined the expression of the microRNAs and found that *miR124*, a direct target of Gli2 (*28*), was significantly down-regulated in *Kif7*$^{-/-}$ ENCCs in our bulk RNA-seq data and as revealed by RT-qPCR (Fig. 5F). Retarded neuronal differentiation of *Kif7*$^{-/-}$ ENCCs was observed at day 5 of differentiation, as induced by addition of glial cell–derived neurotrophic factor (GDNF), and significantly more *Kif7*$^{-/-}$ ENCCs remained as BPs (Phox2b^{+}/Sox10^{+}), accompanied by reduced percentages of NP (Phox2b^{+}/Sox10^{-}) and Tuj1-expressing cells (Fig. 5G). Intriguingly, overexpression of *miR124* enhanced cell progression of *Kif7*$^{-/-}$ ENCCs and greatly improved the neuronal differentiation (Fig. 5, G and H).

Reconstruction of differentiation paths of ENCCs reveals enhancer of Ezh2 as a key regulator of neuronal and glial lineage commitment

To further delineate how Kif7 controls the neuronal differentiation of ENCCs, we analyzed the single-cell transcriptomes of ENCCs and built and compared the differentiation trajectories of the control and *Kif7* mutant cells. E13.5 represents a key window for early ENS development in mice, where two distinct differentiation paths of ENCCs for the neuronal and glial lineages were clearly established (*29*, *30*). Mouse ENCCs and their derivatives were fluorescence-activated cell sorting (FACS)–enriched from E13.5 control (*Wnt1-Cre*;*Rosa26*^{YPF}) and *Kif7* mutant (*Wnt1-Cre*;*Kif7*$^{f/f}$;*Rosa26*^{YPF}) embryonic guts. In total, 7671 control and 15,522 mutant ENCCs were sequenced using Chromium system (10X Genomics), a high-throughput and parallel droplet–based single-cell RNA-seq (scRNA-seq) platform, with 2630 median genes and 9929 mean unique molecular identifiers per cell (fig. S3, A to C). All the single cells were projected on t-distributed stochastic neighbor embedding (t-SNE) plots, and five transcriptionally distinct clusters were identified in both control and mutant ENCCs (Fig. 6A and fig. S3D). The five distinct clusters comprised two distinctive differentiation branches, corresponding to the neuronal and glial lineages. Both paths started at the BP, and the cells on the neuronal differentiation

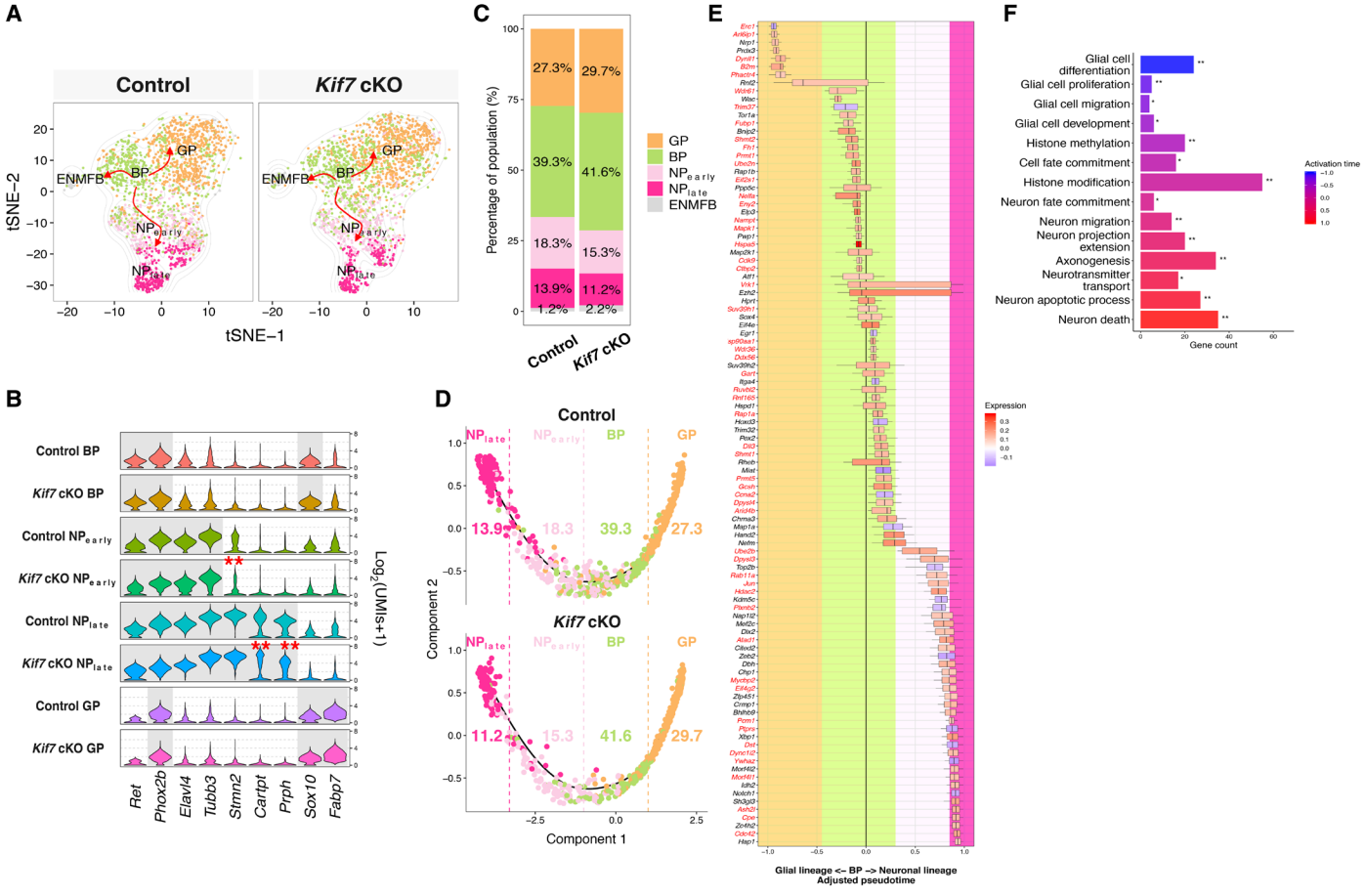

Fig. 6. Reconstruction of the differentiation trajectories of ENCCs reveals Ezh2-mediated core genes underlying neurogenic and gliogenic lineage differentiation. (**A**) t-SNE projection of control and *Kif7* cKO mutant cells during the ENCC differentiation process, colored by inferred cell types (GP, glial progenitor; BP, bipotent progenitor; NP$_{early}$, neuronal progenitor at early stage; NP$_{late}$, neuronal progenitor at late stage; ENMFB, enteric mesothelial fibroblast). (**B**) Violin plot displaying the expression of representative markers in indicated cell types. Significant expression of the genes was labeled with gray color in the background. DEGs are marked by *. (**C**) Bar plot shows the population structure difference between control and *Kif7* cKO mutant cells. (**D**) Trajectory reconstruction of all single cells throughout ENCC differentiation reveals two choices of the BPs. (**E**) Transcriptomic timing analysis of the core gene set of 102 genes along the adjusted ENCC differentiation path. Boxes indicate the period that genes were up-regulated (red) or down-regulated (blue) in *Kif7* cKO mutant cells. The background color indicated the estimated boundaries that separated the cell types. *Ezh2* putative target genes were labeled in red. (**F**) GO analyses of the core gene set of 102 genes. The activation time of each GO term was calculated on the basis of the transcriptomic timing analysis in (E).

trajectory passed through a neuronal intermediate that expressed the early neuronal markers (NP_{early}: *Tubb3*^{high}/*Elavl4*^{high}/*Cartpt*$^{-}$/*Prph*$^{-}$) before they terminated at a more mature state expressing the late neuronal markers (NP_{late}: *Tubb3*^{high}/*Elavl4* ^{high}/*Cartpt*$^{+}$/*Prph*$^{+}$) (Fig. 6B). As for the glial lineage differentiation trajectory, the GPs (*Sox10*^{high}/*Fabp7* ^{high}) were emerging at this stage (Fig. 6, A and B; fig. S3, E and F; and table S1). Another distinct population of progenitors was found to express unique marker set corresponding to the enteric mesothelial fibroblasts (ENMFBs), as previously described (*31*). Although the comparable neuronal and glial lineage differentiation trajectories were found in the control and *Kif7* mutants, a fewer number of neuronal cells were found in *Kif7* mutants (Fig. 6, C and D). To reconstruct a pseudotrajectory of the ENCC differentiation with higher convergence, we ranked cells in a pseudotemporal manner using Monocle 3 after excluding the ENMFB cells (*32*). The trajectory established by Monocle 3 was consistent with the t-SNE plot, confirming the two trajectories of ENCCs from BP to glial cells and neuronal cells. A shift from the neuronal to glial lineage was clearly observed (Fig. 6D and fig. S4), suggesting that Kif7 is involved in the early stages of ENCC differentiation, probably at the stage determining the neuronal versus glial lineage commitment.

We next sought to understand whether and how Kif7 mediates the neuronal and glial lineage commitment by identifying a core set of genes implicated in this process. To this end, we first defined the DEGs in BP, GP, or NP by comparing the control and *Kif7* cKO cells using SCDE [at 5% false discovery rate (FDR)] (table S2). In parallel, we also identified the DEGs across pseudotrajectory of both neuronal and glial lineage using Switchde (at 5% FDR) (table S3). The intersection of these two DEG sets represented the core gene set that plays critical roles in the lineage commitment and Kif7-mediated neurogenic and gliogenic differentiation. The core set contained 102 genes, 16 of which were consistently down-regulated and 86 of which were consistently up-regulated in *Kif7* cKO mutant cells (Fig. 6E). Within the set of 102 DEGs, we found that the regulation periods of *Vrk1* [vaccinia-related kinase (VRK) serine/threonine kinase 1] and *Ezh2* spanned across the early bipotent stage and along the whole neuronal lineage differentiation (Fig. 6E). Intriguingly, we found that most of the genes in the core gene set were the direct targets of Ezh2 based on a public chromatin immunoprecipitation sequencing (ChIP-seq) dataset in a similar tissue from Cistrome database (Fig. 6F, highlighted in red) (*33*, *34*), suggesting that Ezh2 is the key regulator of the core gene set. On the basis of the STRING and GO databases, all these Ezh2 targets interacted with each other and mediated various cellular processes along the neuronal and glial lineage differentiation trajectories, including "histone methylation" and "histone modification" during the early stage of differentiation; "neuron fate commitment", "neuron migration," and "neuron projection" at the intermediate state of neuronal lineage differentiation; and "neuron apoptotic process" and "neuron death" processes at the mature state of neuron (Fig. 6F and fig. S5).

Reduced Gli2 dosage rescues the ENS defects in Kif7 cKO mutants by mediating Ezh2 expression

We have demonstrated that loss of *Kif7* led to up-regulation of Gli2 with concomitant reduction of *miR124,* while overexpression of *miR124* rescued the neuronal differentiation defects of *Kif7*$^{-/-}$ ENCCs. Given that *miR124* has been shown to control the choice between neuronal and astrocyte differentiation by fine-tuning *Ezh2* expression (*22*), it raised an important possibility that Gli2, through *miR124* and Ezh2, regulates the neuronal and glial lineage differentiation of ENCCs in *Kif7* cKO mice.

We next sought to examine the roles of Ezh2 during the neuronal and glial lineage commitment by analyzing its dynamic expression pattern along the differentiation trajectories of ENCCs. We integrated two public scRNA-seq datasets (*31*, *35*) with our scRNA-seq data of wild-type ENCCs collected from E13.5 and E16.5 mouse embryonic guts, as described previously (*29*). All integrated cells from multiple developmental stages were classified into three populations (BP, NP, and GP) on the basis of their expression of canonical markers, as described above. We then determined the relative expression levels of *Ezh2* in NP and GP by comparing to that in BP. The result showed that *Ezh2* was consistently up-regulated in the glial lineage but down-regulated in neuronal lineage at eight different developmental stages (E9.5 to E16.5 and P19 to P21) (Fig. 7A). These data suggest that Ezh2 might play opposing roles in the neuronal and glial lineages. Ezh2 serves as an activator by direct binding onto the promoter/enhancer of its target genes; conversely, it forms a PRC2 complex with Suz12 and Eed to repress gene expression by promoting histone methylation (*18*, *19*). Therefore, we further examined how these functions of Ezh2 regulate the neurogenic and gliogenic lineage differentiation of ENCCs. We applied a three-step strategy; we first compared the correlation between *Ezh2* and every other gene in control and *Kif7* cKO ENCCs to determine whether the regulatory architecture of Ezh2 was significantly altered after the loss of *Kif7* (Fig. 7B). If the expressions of Ezh2-mediated genes were not affected by the loss of *Kif7*, these genes should be located at the diagonal line. However, a global shift of Ezh2 correlation against the diagonal line was observed. This suggests that the expressions of a set of genes have been changed along with Ezh2 after the loss of *Kif7*. Among these genes, they could be positively or negatively correlated to *Ezh2* expression, representing Ezh2-activated and repressed genes, respectively, based on the coexpression analysis. We then made use of a public ChIP-seq dataset designed for Ezh2 from a similar cell state available in Cistrome database (*34*) and used the motif enrichment analysis to further identify the direct/indirect binding genes of Ezh2. Last, 291 genes were predicted as the activated target genes of Ezh2, whose expression levels were significantly elevated in *Kif7* cKO ENCCs, including 16 core genes (Fig. 7B, colored in red; core genes were labeled). Using the same approach, 1022 genes were predicted to be repressed by Ezh2, including four core genes (Fig. 7B, colored in blue; core genes were labeled). When we measured PRC2 activity on the basis of the combined expression levels of three PRC2 subunits (Ezh2, Eed, and Suz12), a significantly higher inferred PRC2 activity was found in *Kif7* cKO ENCCs (Fig. 7C), suggesting a potential involvement of the repressive function of Ezh2 in the aberrant lineage switch in *Kif7* cKO mice. We then predicted how these Ezh2-mediated genes are involved in the neuronal and glial lineage differentiation of ENCCs. To this end, we first identified the neuronal- and glial lineage–associated gene sets by comparing the NP and GP to BP in control at E13.5, respectively. The significantly differentially expressed genes in GP and NP were shown in the volcano plot (Fig. 7D). The putative Ezh2-repressed and Ezh2-activated genes were significantly enriched in the gene sets implicated in neurogenesis (enrichment P value $< 1 \times 10^{-16}$) and gliogenesis (enrichment P value $< 1 \times 10^{-25}$), respectively. GO analyses further revealed that these 1022 genes repressed by Ezh2 are involved in mediating synaptic function and axonogenesis (Fig. 7E).

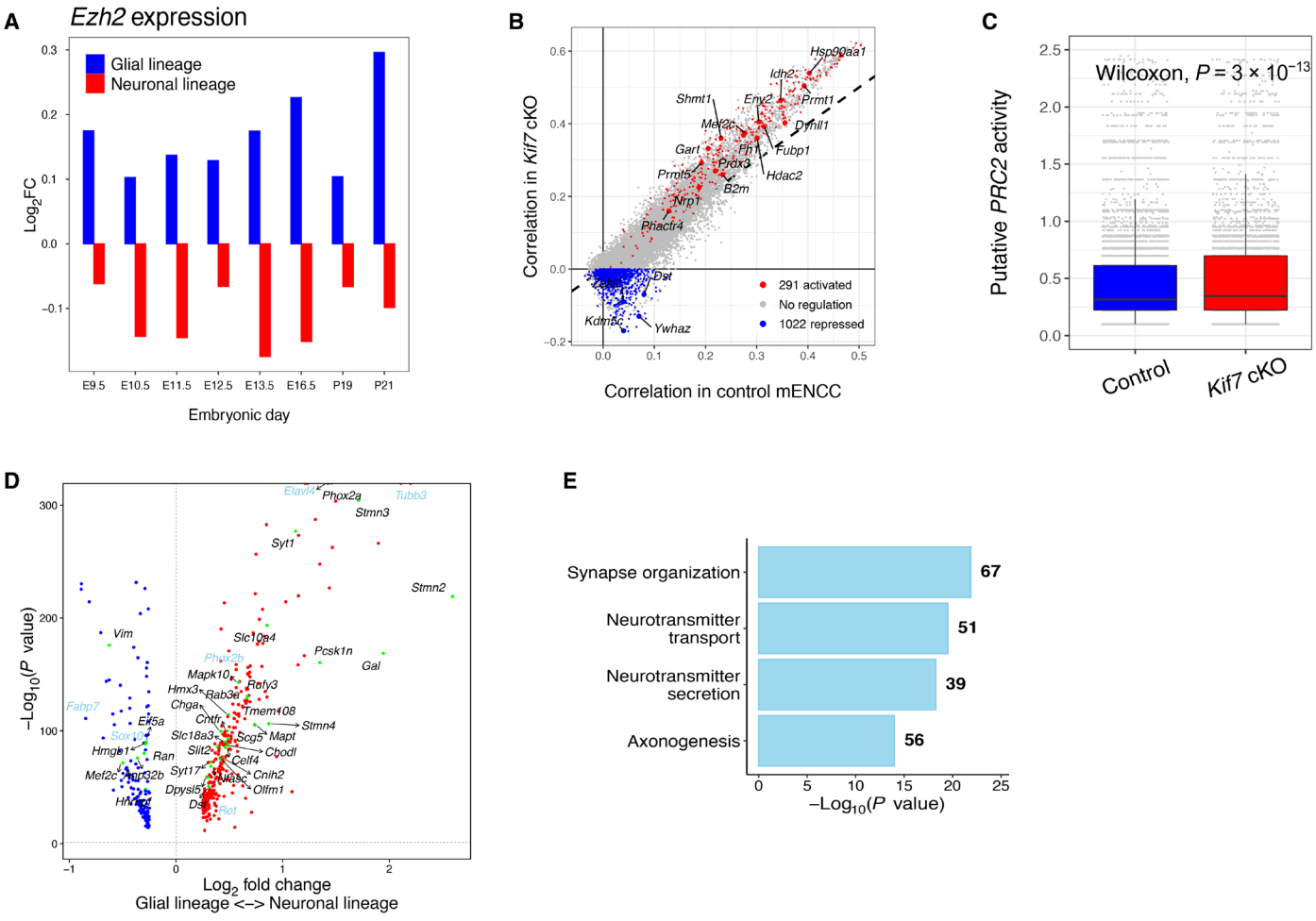

Fig. 7. Single-cell transcriptomic analysis reveals the dual roles of Ezh2 in neurogenic and gliogenic lineage differentiation. (**A**) Bar plot showing the relative expression levels of *Ezh2* during glial and neuronal lineage commitment at multiple developmental stages (E9.5 to E16.5 and P19 to P21) when compared to that in BPs. (**B**) Correlation analysis combined with motif enrichment and differential expression analysis for identification activated (red dots) and repressed (blue dots) target genes of *Ezh2* in control and *Kif7*$^{-/-}$ ENCCs. Genes presented in the core gene set are shown in the scatterplot. (**C**) PRC2 activities in control and *Kif7*$^{-/-}$ ENCCs were assessed by the combined expression level of three subunits: Ezh2, Eed, and Suz12. (**D**) Volcano plot shows that *Ezh2* putative target genes (genes labeled in black, dots in green) in (B) were enriched in the lineage-specific genes (gliogenic lineage–specific genes in blue, neurogenic in red; six known lineage markers were labeled in sky blue). (**E**) *Ezh2 (PRC2)* repressed genes (B) were enriched in GO terms associated with synaptic functions and axonogenesis.

To establish the causal link between Kif7, Gli2, and Ezh2 in neurogenic and gliogenic lineage differentiation of ENCCs, we generated compound mutants with NCC-specific deletions of *Gli2* and *Kif7* (*Wnt1-Cre*;*Kif7*$^{f/f}$;*Gli2*$^{f/+}$). Consistently, Ezh2 expression was significantly elevated in the BP (Ezh2^{high}/Phox2b^{+}/Sox10^{+}, filled yellow arrowheads) and GP (Ezh2^{high}/Phox2b^{-}/Sox10^{+}, filled green arrowheads) of *Kif7* cKO mutants, while deletion of one copy of *Gli2* in *Kif7* cKO mutants reduced the numbers of BP and GP with high Ezh2 expression comparable to those of the control. Unlike in the other two populations, Ezh2 likely forms the PRC2 complex in NP, which makes Ezh2 protein more stable in these cells. Consistently, almost half of NPs expressed high level of Ezh2 (Ezh2^{high}/Phox2b^{+}/Sox10^{-}, filled white arrowheads) in both control and *Kif7* cKO mutants, while upon deletion of *Gli2*, significantly more NPs were found and they stably expressed Ezh2 (Fig. 8A). The increased percentage of Ezh2^{high} NPs in *Wnt1-Cre*;*Kif7*$^{f/f}$;*Gli2*$^{f/+}$ would be the result of the increased numbers of NP and the high stability of Ezh2 protein in these cells. Therefore, we sought to further demonstrate the repressive role of Ezh2 in the neuronal differentiation of ENCCs by directly using the in vitro differentiation assay with two catalytic Ezh2 inhibitors (EPZ-6438 or GSK126) that specifically abolish the PRC2-dependent repressor function of Ezh2, while its transcription activator function remains unaffected (*20*). Addition of these two Ezh2 inhibitors could greatly improve the neuronal differentiation of *Kif7*$^{-/-}$ ENCCs, accompanied by a significant reduction of BP population (Fig. 8B), suggesting that the elevated Ezh2 repressor activity likely inhibits the neuronal differentiation of ENCCs in *Kif7* cKO mutants. We then quantified the uncommitted ENS progenitors, neurons, and glia in the guts of control, *Kif7* cKO, and *Wnt1-Cre*;*Kif7*$^{f/f}$;*Gli2*$^{f/+}$ mice. A robust increase in the number of Sox10^{+}/Ret^{+} uncommitted ENS progenitors and a concomitant reduction in the number of enteric neurons were observed in E13.5 *Kif7* cKO guts. Heterozygous deletion of *Gli2* in *Kif7* cKO mice rescued the population size of the enteric neurons (Fig. 8C) and the

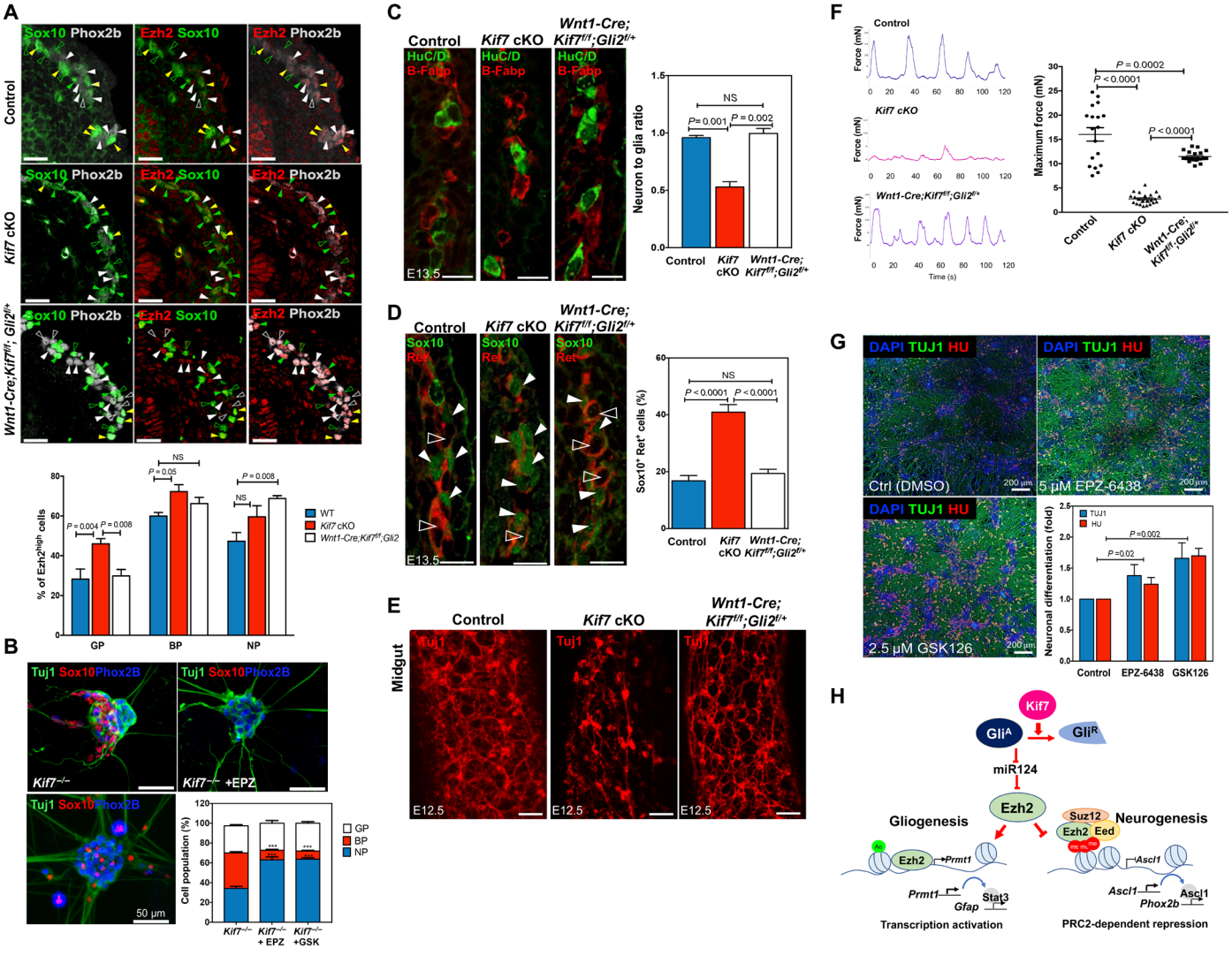

Fig. 8. Kif7-Gli2-Ezh2 mediates the differentiation of mouse and human ENCCs. (**A**) Ezh2 expression in various ENS progenitor pools in E13.5 control and mutant guts. GP, Ezh2^{high}/Sox10^{+}/Phox2b^{-} (green filled arrowheads); BP, Ezh2^{high}/Sox10^{+}/Phox2b^{+} (yellow filled arrowheads); NP, Ezh2^{high}/Sox10^{-}/Phox2b^{+} (white filled arrowheads). Cells with low expression level of Ezh2 are marked with open arrowheads. Bar chart shows the percentages of Ezh2^{high} cells in different ENS progenitor pools ($n = 6$; scale bars, 50 μm). (**B**) In vitro differentiation assay with *Kif7*$^{-/-}$ ENCCs treated with GDNF alone or in combination with either EPZ-6438 or GSK126 for 10 days. Sox10^{+}/Phox2b^{+}, Phox2b^{+}Sox10^{-}, Sox10^{+}/Phox2b^{-}, and Tuj1^{+} cells represent BP, NP, GP, and committed neurons, respectively. Bar chart shows mean ± SEM ($n = 3$). (**C**) Neuronal (HuC/D^{+}) and glial (B-Fabp^{+}) cells, (**D**) progenitors (Ret^{+} Sox10^{+}, filled arrowheads), and neuronal precursors (Ret^{+} Sox10^{-}, open arrowheads) in E13.5 control and mutant guts were detected using immunohistochemistry. The neuron-to-glia ratios and the percentages of Sox10^{+} Ret^{+} cells over the sum of Ret^{+} and Sox10^{+} cells are shown in the bar charts ($n = 6$; scale bars, 25 μm). (**E**) Whole-mount immunostaining with Tuj1 antibody. Scale bars, 100 μm. (**F**) Gut motility assay with the distal colon of control and mutants. Dot plot shows the maximum contraction force detected in the control and mutants ($n = 6$). (**G**) hENCCs were cultured in neuronal differentiation for 5 days in the absence or presence of Ezh2 inhibitor (GSK126, 2.5 μM or EPZ-6438, 5 μM). The differentiation capacities of hENCCs were monitored on the basis of the expressions of TUJ1/HU, as revealed by immunocytochemistry. Bar charts show mean ± SEM ($n = 3$). (**H**) Schematic shows the regulatory network of Kif7-Gli2-*miR124*-Ezh2 underlying the neurogenic and gliogenic lineage differentiation.

uncommitted ENS progenitors (Fig. 8D). With respect to the organization of the neuronal network, the impaired directional migration in *Kif7* cKO ENCCs resulted in abnormal organization of the neuronal network, with fewer neuronal cell bodies and Tuj1^{+} neural projections in the midguts of the animals. Both the density and the distribution of neuronal cell bodies and their processes in the compound mutants (*Wnt1-Cre;Kif7*$^{f/f}$*;Gli2*$^{f/+}$) were found to be comparable to the control (Fig. 8E). Loss of one allele of *Gli2* in *Kif7* mutants almost completely rescued both the survival and the intestinal motility. All the *Wnt1-Cre;Kif7*$^{f/f}$*;Gli2*$^{f/+}$ mutants could survive with no obvious ENS defect. We also analyzed the gut contractility of the distal colon of the mutants. The contraction patterns in response to the low-voltage electrical field stimulation were highly comparable between control and *Wnt1-Cre;Kif7*$^{f/f}$*;Gli2*$^{f/+}$ mutants, while *Kif7* cKO mutant colon failed to induce gut contraction (Fig. 8F). Together, the expression of Ezh2 is elevated in GP and BP ENCC populations in *Kif7 cKO* mutants and is caused by the up-regulation of Gli2, and that led to the suppression of the ENCC differentiation accompanied

by an aberrant up-regulation of genes implicated in gliogenesis, resulting in a reduced NP population in *Kif7 cKO* mutants. Ezh2 protein is likely highly stable in NPs and works as a PRC2-dependent repressor to inhibit neurogenesis of ENCCs. Reducing the Ezh2 expression level in BPs of *Kif7 cKO* mutants by deletion of one copy of *Gli2* or inhibition of the repressor function of Ezh2 could rescue the neurogenic lineage differentiation defect of $Kif7^{-/-}$ ENCCs.

We then compared the neuronal differentiation trajectory of mouse ENCCs with that of the human ENCCs (hENCCs), which were derived from human induced pluripotent stem cells (hiPSCs), as described previously (*29*, *36*). Among the core gene set of 102 genes, 51 genes showed significant (22 up- and 29 down-regulated, $P < 0.05$) and consistent dynamic expression along the human and mouse neuronal lineage differentiation trajectories as inferred by the pseudotime analysis (fig. S7). This result indicated that the regulatory network among the EZH2-mediated core gene set is likely conserved among human and mouse. To directly demonstrate whether inhibition of EZH2 can promote the neurogenesis of hENCCs, we used hiPSC to model the development of human ENS. hENCCs were first derived from a hiPSC line using a dual-SMAD inhibition protocol in the presence of retinoic acid and enriched with antibodies against HNK1 and $p75^{NTR}$, as described previously (*29*, *36*). The hENCCs were then directed to neuronal lineage to generate enteric NPs. In concordant with in silico prediction, inhibition of EZH2, by addition of EZH2 inhibitor (GSK126 or EPZ-6438), favored the neuronal lineage differentiation of hiPSC-derived ENCC, and significantly more TUJ1- and HU-expressing NPs were found at day 5 of differentiation (Fig. 8G). Therefore, EZH2-mediated ENCC differentiation is largely conserved among mouse and human.

DISCUSSION

The ENS defects in *Kif7* cKO have highlighted the relevance of the timely coordination between migration and differentiation of ENCCs and the development of gut mesenchyme in the proper development of ENS. Loss of *Kif7* causes defects not only in the ENCC differentiation but also in its migration. The migration defect of *Kif7* cKO ENCCs perturbs the development of both submucosal and myenteric plexuses. The erratic migratory pattern of the mutant ENCCs leads to a delayed colonization of the gut at E12.5. Although ENCCs can fully colonize the whole gut in *Kif7* mutants by E15.5 for the subsequent formation of the myenteric neurons and glia, the erratic migratory pattern of the mutant ENCCs leads to uneven distribution of neurons and glia along the bowel, resulting in disorganized myenteric ganglia, as seen in *Kif7* cKO adult mice. In addition, the migration defect may also lead to the marked reduction of progenitor pool size at the submucosal layer and interfere with the subsequent formation of submucosal plexus. Given that loss of *Kif7* also significantly reduces the neuronal precursor ($Tuj1^{+}$) (Fig. 3B), the number of late-born inhibitory neurons is substantially reduced in myenteric plexuses.

At the molecular level, we establish here that Kif7 negatively regulates Gli2 and Ezh2 in such a way as to prevent aberrant activation of the Hedgehog pathway. Low Gli activity is required for neuronal lineage differentiation and maintains the expression of *miR124* to reduce the expression level of Ezh2 and its repression on the neurogenesis mediators (*Ascl1*, *Phox2a*, and *Phox2b*). PRC2-dependent repressor function of Ezh2 down-regulates the expression of neuronal genes, while Ezh2 also serves as the transcription activator to up-regulate the expressions of some glial genes such as Prmt1-Stat3, favoring the glial fate differentiation (Fig. 8H). Loss of *Kif7* disrupts the Gli2-Ezh2–mediated cell state progression, neuronal lineage differentiation of ENCCs, and axonogenesis, resulting in malformation of ENS.

Kif7 can positively and negatively regulate the Hedgehog pathway in different cellular contexts (*37*–*40*). Most of the features of the ENS phenotypes in *Kif7* cKO mutants described here can be explained by the increased levels of Gli activator (Gli^{A}), and these phenotypes can be rescued by deletion of one allele of *Gli2*. This is consistent with the established role of Kif7 in ventral neural tube patterning (*24*), and Gli proteins act as prominent positive regulators without an obvious negative regulatory role in Hedgehog signaling, a feature that may reflect an NCC-specific function of Kif7. This observation is consistent with our earlier findings in *Ptch1* (*6*) and *Sufu* (*4*) cKO mutants, in which Hedgehog signaling is consecutively activated with elevated expression of Gli^{A}, and both result in premature glial lineage differentiation, leading to reduced neuron-to-glia ratio in their ENS at E12.5. Unlike the *Ptch1* and *Sufu* cKO mutants, Sox10 is down-regulated in ENCCs of *Kif7* mutants, *Kif7*-deficient ENCCs mainly exhibit defects in neuronal differentiation and migration, and we find no evidence of expansion of the glial population when Hedgehog is activated by deletion of *Kif7*. As revealed by scRNA-seq analysis of ENCCs from a Gli-reporter (*GBS-GFP*) mouse line, Hedgehog pathway is activated mainly in the BP population but not in the committed populations (*29*). Together with the findings from the current study, Hedgehog likely takes an active role in controlling differentiation of ENCCs. The level of Gli^{A} is likely involved in mediating cell state progression of ENCC and their subsequent neuronal differentiation, while its role on gliogenesis relies mainly on the presence of other key glial mediators, such as Sox10.

Because bulk RNA-seq acquires only snapshots of transcriptomes of the mutant cells, it is still challenging to identify the key molecular drivers for the phenotypic changes as observed in mice. Therefore, we made use of transcriptomic data generated by high-resolution RNA-seq to build the differentiation trajectories to reveal the molecular perturbations along various cellular states in the mutants. One of our central findings is that loss of *Kif7* disturbs the lineage commitment of ENCCs. More mutant ENCCs remain as undifferentiated and fail to progress to the neuronal lineage, with a differentiation bias toward the glial lineage. As a result, the number of neurons is significantly reduced in *Kif7* mutants. Therefore, by comparing the DEGs identified along the pseudotime of development and between the control and *Kif7* mutant cells, 102 genes were identified as the core gene sets mediating the neuronal versus glial lineage commitment and cell progression along the committed lineages. Subsequent analyses further identified Ezh2 as a direct regulator of 54 of these 102 core genes, suggesting that Ezh2 likely serves as a master regulator underlying this cellular process.

Ezh2 has dual regulatory roles in gene transcription, so it can mediate a large number of genes and control various cellular processes. In ENCCs, the activator function of Ezh2 is crucial for glial lineage differentiation. Ezh2 itself and most of Ezh2 positively associated genes are on the glial lineage differentiation path (Fig. 7, A and D). For instance, *Prmt1* is a direct target of Ezh2 and is up-regulated in *Kif7* cKO. Prmt1 methylates arginine residue(s) of signal transducer and activator of transcription 3 (Stat3) to positively regulate its activity, promoting the astrocytic differentiation of neural

stem cells (*41*). On the other hand, Ezh2 is a core component of PRC2 complex and suppresses gene transcription by promoting histone methylation. Given a significantly higher inferred PRC2 activity observed in *Kif7* cKO ENCCs, Ezh2-associated gene suppression should also contribute to the ENS phenotypes as seen in *Kif7* cKO mutants. In concordant with this observation, many of Ezh2 negatively associated genes are implicated in the neurogenic lineage differentiation. Although the aberrantly high Ezh2-associated PCR2 activity suppresses the neurogenic lineage differentiation of ENCCs, expression of Ezh2 is essential for the cell state progression of ENCCs to initiate the cellular differentiation. Genetic ablation of *Ezh2* in NCC disrupts the formation of ENS with aberrant up-regulation of numerous NC-associated genes (*Zic1*, *Pax3*, and *Sox10*) (*42*). On the basis of our data, the dynamic and timely control of the expression level of Ezh2 along the neuronal and glial lineages is critical for ENCC development. High expression level of Ezh2 is required for the initiation of cell progression and glial lineage differentiation, while suppression of Ezh2 favors the cell progression along the neuronal differentiation path. These data highlight the relevance of both transcriptional and epigenetic control in early development of ENCCs.

How Hedgehog regulates the neurogenic and gliogenic lineage differentiation of ENCCs has remained a mystery. Here, we define the molecular regulation of Ezh2 by Hedgehog signaling, and it likely represents the major mechanism accounting for neurogenic and gliogenic lineage differentiation mediated by Hedgehog pathway. In *Kif7* cKO ENCCs, the aberrantly high Gli^A results in the elevated expression of Ezh2, and that can be rescued by deletion of a copy of *Gli2*. Instead of inducing the transcription of *Ezh2*, Gli^A works by suppressing the expression of *miR124*, where *miR124* is a direct target of Gli2 (*28*), and it negatively regulates *Ezh2* expression (*22*). Consistently, overexpression of *miR124*, inhibition of Ezh2, or deletion of a copy of *Gli2* can nicely correct the differentiation defects of *Kif7* cKO ENCCs.

With regard to human diseases, mutations in the genes encoding various components of the Hedgehog signaling pathway have been reported in patients with ciliopathies (*14*) and HSCR disease (*4*, *6*), and KIF7 has been causally associated with various ciliopathies (*15*). Nevertheless, the genetic basis of non-HSCR gastrointestinal dysmotility is complex and likely heterogeneous, so it is still difficult to establish disease causality in which a given gene accounts for both the gastrointestinal dysmotility and ciliopathies. Our data from the mouse study suggest that defective KIF7/Hedgehog signaling may represent one of the primary causes underlying ciliopathies and gastrointestinal motility disorders. *Kif7* null mice display multisystemic ciliopathy–associated phenotypes, while NCC-specific conditional *Kif7* cKO mice exhibit gastrointestinal dysfunction, resulting in retarded growth at the neonatal stage, which mirrors the phenotypes seen in patients with CIPO/ED. On the basis of the ENS phenotypes of various mouse mutants, it is conceivable that individuals harboring mutations in different Hedgehog pathway genes would experience different phenotypic severities and comorbidities, manifesting the broad phenotypic spectra of the disorders. In addition, the Ezh2-mediated core regulatory network underlying ENCC differentiation is highly conserved among human and mouse. Therefore, the involvement of Ezh2-mediated core regulatory network in various ENS defects deserves further study.

In summary, we have demonstrated that ENS development is precisely regulated by the level of Gli^A and Ezh2, which determines the pool size of the neuronal precursors for the generation of a functional ENS with full neuronal diversity. Mutations in various components of the Hedgehog signaling system may alter Gli^A levels. This represents a common underlying pathogenic mechanism that can account for a broad range of manifestations and severity in ciliopathy patients with gastrointestinal motility disorders ranging from HSCR to CIPO/ED.

MATERIALS AND METHODS

Mice

Wnt1-Cre, $Rosa26^{YFP}$ (*R26R-EYFP*), and $Gli2^{f/+}$ and $Kif7^{f/+}$ mice were maintained in a mixed outbred background of C57 and 129/S6 at the Animal Laboratory of the University of Hong Kong. All experiments were performed in accordance with procedures approved by the Committee on the Use of Live Animals, the University of Hong Kong (CULTRA 3792-15).

Spatiotemporal mapping of colonic motility

The colons of 3- to 4-week-old *Kif7* KO mice and those of their control littermates were dissected out, pinned to a chamber through which a flow of oxygenated physiological saline solution was maintained, and equilibrated at 37°C for 30 min. Mouse stool was then inserted into the oral end of the colon, and time-lapse cinematography of gut motility was performed at 30 frames/s using a digital camera (Stylus Tough, Olympus Inc.). The video recordings were converted into spatiotemporal plots using ImageJ software and used to characterize the CMMCs, which constitute the recurrent ENS-mediated contractions propagating along the colon preparations. Stool movement speed was calculated as the time required to expel a fecal pellet inserted at the oral end of the colon preparation from its anal end divided by the length of the colon preparation. At least six samples from each experimental group were examined; the mean values of stool movement speed ± SEM are shown in the bar charts.

Adult myenteric plexus preparation and immunostaining

The colons and ilea of 3- to 4-week-old mice were removed by dissection. The mucosal layer was removed from the muscle layers containing the myenteric plexus using forceps with an extremely fine point. Myenteric plexus segments were permeabilized and blocked with 10% fetal bovine serum (FBS) before incubation with primary antibodies (anti-S100β, anti-GFAP, anti-nNOS, anti-calretinin, anti-Tuj1, and/or anti-HuC/D) and donkey secondary antibodies (Alexa Fluor 488, 594, or 647).

Immunofluorescence

Embryos and guts were fixed in 4% paraformaldehyde and dehydrated and embedded in OCT (optimal cutting temperature) (Tissue-Tek). For immunohistochemistry, the sections were blocked with 10% normal goat serum or FBS before incubation with primary antibodies. Lists of the primary and secondary antibodies and the working dilutions used are provided in tables S4 and S5, respectively.

Gut explant cultures and time-lapse imaging

For gut migration studies, the guts of E12.5 mouse embryos of the $Rosa26^{YFP}$ genetic background were dissected. The whole guts were placed on filter paper (Millipore, Billerica) and cultured in Dulbecco's modified Eagle's medium containing 10% FBS in a heat- and humidity-controlled chamber at 5% CO_2 and 37°C. Images were

captured using a Carl Zeiss LSM 800 laser scanning confocal microscope. Individual ENCCs in gut explants were tracked using ImageJ software to determine their migration speed and persistence of movement. The speed of migration was determined by dividing the length of the trajectory by the time of migration (a minimum of 14 hours of transport was measured). The net speed of each cell was determined by dividing the distance between the start and end points by the time required to traverse that distance. Persistence was determined by dividing the distance between the initial and final positions by the total distance covered by the cell.

Flow cytometry analysis

For flow cytometry analysis, E13.5 embryonic guts were dissociated using dispase I and collagenase. The dissociated cells were then incubated with antibodies against integrin 4α and $p75^{NTR}$ (table S4) for 30 min at 4°C. Approximately 10^6 labeled cells were acquired and analyzed using a FACSCalibur cell sorter (Becton Dickinson Immunocytometry Systems). Cells labeled with isotype-matched nonspecific immunoglobulins were used as controls. FlowJo software version 8.2 (Tree Star Inc.) was used to analyze flow data.

Mouse ENCC culture and viral transduction

ENCCs were isolated from E11.5 *Kif7*$^{f/f}$ embryonic guts and enriched by multiple replating, as previously described (*4*). The ENCCs were transduced with Ad-GFP and Ad-Cre-GFP recombinant adenoviruses to generate control and *Kif7*$^{-/-}$ ENCCs, respectively. Deletion of *Kif7* and activation of hedgehog signaling were confirmed by RT-PCR and Western blotting, respectively.

Derivation of hENCC from hPSCs and neuronal differentiation

hENCCs were derived from human pluripotent stem cell (hPSCs) and then directed to neuronal lineage for generation of human enteric NPs, as described previously (*29*, *36*, *43*). To examine the effect of Ezh2 on neuronal differentiation of hENCCs, hENCCs were cultured in differentiated medium [N2 medium containing brain-derived neurotropic factor (BDNF) (10 ng/ml; PeproTech), GDNF (10 ng/ml; PeproTech), NT-3 (10 ng/ml; PeproTech), nerve growth factor (NGF) (10 ng/ml; PeproTech), 1 μM dibutyryl adenosine 3′,5′-monophosphate (cAMP) (Sigma-Aldrich), and 200 μM ascorbic acid (Sigma-Aldrich)] in the absence or presence of Ezh2 inhibitor (GSK126, 2.5 μM, Abcam or EPZ-6438, 5 μM, AbMole) for 5 days. The differentiation capacity of hENCCs was monitored on the basis of the expressions of TUJ1/HU, as revealed by immunocytochemistry.

Immunoblot

Fifty micrograms of total protein lysates from control and *Kif7*$^{-/-}$ ENCCs was separated on 8% SDS–polyacrylamide gels and transferred to polyvinylidene fluoride membranes. The membranes were incubated with antibodies against Gli1, Gli2, and Gli3. Anti–β-actin was used as a loading control (tables S4 and S5). Antibody-bound proteins were visualized using the Western Bright ECL HRP substrate (Adavansta).

Quantitative reverse transcription polymerase chain reaction

Total RNA was extracted from control and *Kif7*$^{-/-}$ ENCCs using the RNeasy Mini Kit (Qiagen) and reverse-transcribed in a 10-μl reaction system using the PrimeScript RT Master Mix (Takara) to generate complementary DNA (cDNA) according to the manufacturer's instructions. Quantitative PCR was performed using the SYBR Green qPCR Kit (Applied Biosystems) and the ABI 7900HT Fast Real-Time PCR System (Applied Biosystems). The primer information is listed in table S6. Ribosomal 18S RNA was used as an internal control. The values reported in the bar charts represent the mean ± SEM of the values obtained in experiments that were repeated in three independent assays.

RNA sequencing

RNA-seq of RNA obtained from control and *Kif7*$^{-/-}$ ENCCs was performed at the Centre of Genomic Science, the University of Hong Kong. The detailed methods used in RNA-seq data analysis are provided in the Supplementary Materials.

Droplet-based scRNA-seq

Droplet-based scRNA-seq was performed at the Centre of Genomic Science, the University of Hong Kong. For scRNA-seq of mouse ENCCs, GemCode single-cell platform based on the GemCode gel bead was used to process the single cells. Chip and Library Kits (10X Genomics, Pleasanton) were used according to the manufacturer's protocol. In brief, ENCCs were enriched by cell sorting, and enriched cells were partitioned into gel beads in emulsion in the GemCode instrument, followed by cell lysis and barcoded reverse transcription of RNA. Last, amplification, shearing, and 5′ adaptor and sample index attachment were performed. Libraries were purified and sequenced on Illumina NextSeq 500, as described above. The detailed methods used in RNA-seq data analysis are provided in the Supplementary Materials.

Statistical analysis

The differences among multiple treatment groups were analyzed with a two-sided unpaired Student's *t* test or one-way analysis of variance followed by Tukey post-test using GraphPad Prism 7 (GraphPad Software). A *P* value less than 0.05 was interpreted to represent a statistically significant difference. All experiments were replicated at least three times, and data are shown as means with SEM.

Study approval

All experiments were performed in accordance with procedures approved by the committee on the Use of Live Animals, the University of Hong Kong (CULTRA 3792-15).

SUPPLEMENTARY MATERIALS

Supplementary material for this article is available at https://science.org/doi/10.1126/sciadv.abf7472

View/request a protocol for this paper from *Bio-protocol*.

REFERENCES AND NOTES

1. M. L. Westfal, A. M. Goldstein, Pediatric enteric neuropathies: Diagnosis and current management. *Curr. Opin. Pediatr.* **29**, 347–353 (2017).
2. T. A. Heanue, V. Pachnis, Enteric nervous system development and Hirschsprung's disease: Advances in genetic and stem cell studies. *Nat. Rev. Neurosci.* **8**, 466–479 (2007).
3. M. Nagashimada, H. Ohta, C. Li, K. Nakao, T. Uesaka, J. F. Brunet, J. Amiel, D. Trochet, T. Wakayama, H. Enomoto, Autonomic neurocristopathy-associated mutations in PHOX2B dysregulate *Sox10* expression. *J. Clin. Invest.* **122**, 3145–3158 (2012).
4. J. A.-J. Liu, F. P.-L. Lai, H.-S. Gui, M.-H. Sham, P. K.-H. Tam, M.-M. Garcia-Barcelo, C.-C. Hui, E. S.-W. Ngan, Identification of GLI mutations in patients with Hirschsprung disease that disrupt enteric nervous system development in mice. *Gastroenterology* **149**, 1837–1848.e5 (2015).
5. J. Mao, B.-M. Kim, M. Rajurkar, R. A. Shivdasani, A. P. McMahon, Hedgehog signaling controls mesenchymal growth in the developing mammalian digestive tract. *Development* **137**, 1721–1729 (2010).
6. E. S.-W. Ngan, M.-M. Garcia-Barcelo, B. H.-K. Yip, H.-C. Poon, S.-T. Lau, C. K.-M. Kwok, E. Sat, M.-H. Sham, K. K.-Y. Wong, B. J. Wainwright, S. S. Cherny, C.-C. Hui, P. C. Sham, V. C.-H. Lui,

P. K.-H. Tam, Hedgehog/Notch-induced premature gliogenesis represents a new disease mechanism for Hirschsprung disease in mice and humans. *J. Clin. Invest.* **121**, 3467–3478 (2011).
7. M. Ramalho-Santos, D. A. Melton, A. P. McMahon, Hedgehog signals regulate multiple aspects of gastrointestinal development. *Development* **127**, 2763–2772 (2000).
8. N. Nagy, C. Barad, H. K. Graham, R. Hotta, L. S. Cheng, N. Fejszak, A. M. Goldstein, Sonic hedgehog controls enteric nervous system development by patterning the extracellular matrix. *Development* **143**, 264–275 (2016).
9. D. Huangfu, A. Liu, A. S. Rakeman, N. S. Murcia, L. Niswander, K. V. Anderson, Hedgehog signalling in the mouse requires intraflagellar transport proteins. *Nature* **426**, 83–87 (2003).
10. K. F. Liem Jr., M. He, P. J. R. Ocbina, K. V. Anderson, Mouse Kif7/Costal2 is a cilia-associated protein that regulates Sonic hedgehog signaling. *Proc. Natl. Acad. Sci. U.S.A.* **106**, 13377–13382 (2009).
11. M. He, R. Subramanian, F. Bangs, T. Omelchenko, K. F. Liem Jr., T. M. Kapoor, K. V. Anderson, The kinesin-4 protein Kif7 regulates mammalian Hedgehog signalling by organizing the cilium tip compartment. *Nat. Cell Biol.* **16**, 663–672 (2014).
12. D. Barakeh, E. Faqeih, S. Anazi, M. S. Al-Dosari, A. Softah, F. Albadr, H. Hassan, A. M. Alazami, F. S. Alkuraya, The many faces of *KIF7*. *Hum. Genome Var.* **2**, 15006 (2015).
13. C. C. Hui, S. Angers, Gli proteins in development and disease. *Annu. Rev. Cell Dev. Biol.* **27**, 513–537 (2011).
14. C. Dafinger, M. C. Liebau, S. M. Elsayed, Y. Hellenbroich, E. Boltshauser, G. C. Korenke, F. Fabretti, A. R. Janecke, I. Ebermann, G. Nurnberg, P. Nurnberg, H. Zentgraf, F. Koerber, K. Addicks, E. Elsobky, T. Benzing, B. Schermer, H. J. Bolz, Mutations in KIF7 link Joubert syndrome with Sonic Hedgehog signaling and microtubule dynamics. *J. Clin. Invest.* **121**, 2662–2667 (2011).
15. R. Purkait, R. Basu, R. Das, U. Chatterjee, Association of Joubert syndrome and Hirschsprung disease. *Indian Pediatr.* **52**, 61–62 (2015).
16. P. F. Laje, S. J. Fenton, W. H. Peranteau, Total colonic Hirschsprung's disease and anorectal malformation in a baby with Pallistere–Hall syndrome. *J. Ped. Surg. Case Rep.* **1**, 308–310 (2013).
17. A. Karaman, Bardet-Biedl syndrome: A case report. *Dermatol. Online J.* **14**, 9 (2008).
18. R. Cao, L. Wang, H. Wang, L. Xia, H. Erdjument-Bromage, P. Tempst, R. S. Jones, Y. Zhang, Role of histone H3 lysine 27 methylation in Polycomb-group silencing. *Science* **298**, 1039–1043 (2002).
19. L. A. Boyer, K. Plath, J. Zeitlinger, T. Brambrink, L. A. Medeiros, T. I. Lee, S. S. Levine, M. Wernig, A. Tajonar, M. K. Ray, G. W. Bell, A. P. Otte, M. Vidal, D. K. Gifford, R. A. Young, R. Jaenisch, Polycomb complexes repress developmental regulators in murine embryonic stem cells. *Nature* **441**, 349–353 (2006).
20. J. Kim, Y. Lee, X. Lu, B. Song, K.-W. Fong, Q. Cao, J. D. Licht, J. C. Zhao, J. Yu, Polycomb- and methylation-independent roles of EZH2 as a transcription activator. *Cell Rep.* **25**, 2808–2820.e4 (2018).
21. D. Zingg, J. Debbache, R. Peña-Hernández, A. T. Antunes, S. M. Schaefer, P. F. Cheng, D. Zimmerli, J. Haeusel, R. R. Calçada, E. Tuncer, Y. Zhang, R. Bossart, K.-K. Wong, K. Basler, R. Dummer, R. Santoro, M. P. Levesque, L. Sommer, EZH2-mediated primary cilium deconstruction drives metastatic melanoma formation. *Cancer Cell* **34**, 69–84.e14 (2018).
22. W. H. Neo, K. Yap, S. H. Lee, L. S. Looi, P. Khandelia, S. X. Neo, E. V. Makeyev, I. H. Su, MicroRNA miR-124 controls the choice between neuronal and astrocyte differentiation by fine-tuning Ezh2 expression. *J. Biol. Chem.* **289**, 20788–20801 (2014).
23. S. J. Deimling, K. Lau, C.-C. Hui, S. Hopyan, Genetic interaction between Gli3 and Ezh2 during limb pattern formation. *Mech. Dev.* **151**, 30–36 (2018).
24. S. Endoh-Yamagami, M. Evangelista, D. Wilson, X. Wen, J. W. Theunissen, K. Phamluong, M. Davis, S. J. Scales, M. J. Solloway, F. J. de Sauvage, A. S. Peterson, The mammalian Cos2 homolog Kif7 plays an essential role in modulating Hh signal transduction during development. *Curr. Biol.* **19**, 1320–1326 (2009).
25. T. G. Bush, N. J. Spencer, N. Watters, K. M. Sanders, T. K. Smith, Spontaneous migrating motor complexes occur in both the terminal ileum and colon of the C57BL/6 mouse in vitro. *Auton. Neurosci.* **84**, 162–168 (2000).
26. T. A. Heanue, V. Pachnis, Prospective identification and isolation of enteric nervous system progenitors using *Sox2*. *Stem Cells* **29**, 128–140 (2011).
27. M. J. Simpson, D. C. Zhang, M. Mariani, K. A. Landman, D. F. Newgreen, Cell proliferation drives neural crest cell invasion of the intestine. *Dev. Biol.* **302**, 553–568 (2007).
28. Z. Yao, L. Han, Y. Chen, F. He, B. Sun, S. Kamar, Y. Zhang, Y. Yang, C. Wang, Z. Yang, Hedgehog signalling in the tumourigenesis and metastasis of osteosarcoma, and its potential value in the clinical therapy of osteosarcoma. *Cell Death Dis.* **9**, 701 (2018).
29. S.-T. Lau, Z. Li, F. Pui-Ling Lai, K. Nga-Chu Lui, P. Li, J. O. Munera, G. Pan, M. M. Mahe, C.-C. Hui, J. M. Wells, E. Sau-Wai Ngan, Activation of hedgehog signaling promotes development of mouse and human enteric neural crest cells, based on single-cell transcriptome analyses. *Gastroenterology* **157**, 1556–1571.e5 (2019).
30. R. Lasrado, W. Boesmans, J. Kleinjung, C. Pin, D. Bell, L. Bhaw, S. McCallum, H. Zong, L. Luo, H. Clevers, P. Vanden Berghe, V. Pachnis, Lineage-dependent spatial and functional organization of the mammalian enteric nervous system. *Science* **356**, 722–726 (2017).
31. A. Zeisel, H. Hochgerner, P. Lönnerberg, A. Johnsson, F. Memic, J. van der Zwan, M. Häring, E. Braun, L. E. Borm, G. La Manno, S. Codeluppi, A. Furlan, K. Lee, N. Skene, K. D. Harris, J. Hjerling-Leffler, E. Arenas, P. Ernfors, U. Marklund, S. Linnarsson, Molecular architecture of the mouse nervous system. *Cell* **174**, 999–1014.e22 (2018).
32. X. Qiu, Q. Mao, Y. Tang, L. Wang, R. Chawla, H. A. Pliner, C. Trapnell, Reversed graph embedding resolves complex single-cell trajectories. *Nat. Methods* **14**, 979–982 (2017).
33. S. Kundu, F. Ji, H. Sunwoo, G. Jain, J. T. Lee, R. I. Sadreyev, J. Dekker, R. E. Kingston, Polycomb repressive complex 1 generates discrete compacted domains that change during differentiation. *Mol. Cell* **65**, 432–446.e5 (2017).
34. T. Liu, J. A. Ortiz, L. Taing, C. A. Meyer, B. Lee, Y. Zhang, H. Shin, S. S. Wong, J. Ma, Y. Lei, U. J. Pape, M. Poidinger, Y. Chen, K. Yeung, M. Brown, Y. Turpaz, X. S. Liu, Cistrome: An integrative platform for transcriptional regulation studies. *Genome Biol.* **12**, R83 (2011).
35. J. Cao, M. Spielmann, X. Qiu, X. Huang, D. M. Ibrahim, A. J. Hill, F. Zhang, S. Mundlos, L. Christiansen, F. J. Steemers, C. Trapnell, J. Shendure, The single-cell transcriptional landscape of mammalian organogenesis. *Nature* **566**, 496–502 (2019).
36. F. P.-L. Lai, S.-T. Lau, J. K.-L. Wong, H. Gui, R. X. Wang, T. Zhou, W. H. Lai, H.-F. Tse, P. K.-H. Tam, M.-M. Garcia-Barcelo, E. S.-W. Ngan, Correction of Hirschsprung-associated mutations in human induced pluripotent stem cells via clustered regularly interspaced short palindromic repeats/Cas9, restores neural crest cell function. *Gastroenterology* **153**, 139–153.e8 (2017).
37. D. Huangfu, K. V. Anderson, Cilia and Hedgehog responsiveness in the mouse. *Proc. Natl. Acad. Sci. U.S.A.* **102**, 11325–11330 (2005).
38. C. J. Haycraft, B. Banizs, Y. Aydin-Son, Q. Zhang, E. J. Michaud, B. K. Yoder, Gli2 and Gli3 localize to cilia and require the intraflagellar transport protein polaris for processing and function. *PLOS Genet.* **1**, e53 (2005).
39. S. R. May, A. M. Ashique, M. Karlen, B. Wang, Y. Shen, K. Zarbalis, J. Reiter, J. Ericson, A. S. Peterson, Loss of the retrograde motor for IFT disrupts localization of Smo to cilia and prevents the expression of both activator and repressor functions of Gli. *Dev. Biol.* **287**, 378–389 (2005).
40. H. O.-L. Cheung, X. Zhang, A. Ribeiro, R. Mo, S. Makino, V. Puviindran, K. K. L. Law, J. Briscoe, C.-C. Hui, The kinesin protein Kif7 is a critical regulator of Gli transcription factors in mammalian hedgehog signaling. *Sci. Signal.* **2**, ra29 (2009).
41. M. Honda, K. Nakashima, S. Katada, PRMT1 regulates astrocytic differentiation of embryonic neural stem/precursor cells. *J. Neurochem.* **142**, 901–907 (2017).
42. H. Kim, I. M. Langohr, M. Faisal, M. McNulty, C. Thorn, J. Kim, Ablation of Ezh2 in neural crest cells leads to aberrant enteric nervous system development in mice. *PLOS ONE* **13**, e0203391 (2018).
43. C. S.-M. Tang, P. Li, F. P.-L. Lai, A. X. Fu, S.-T. Lau, M. T. So, K. N.-C. Lui, Z. Li, X. Zhuang, M. Yu, X. Liu, N. D. Ngo, X. Miao, X. Zhang, B. Yi, S. Tang, X. Sun, F. Zhang, H. Liu, Q. Liu, R. Zhang, H. Wang, L. Huang, X. Dong, J. Tou, K. S.-E. Cheah, W. Yang, Z. Yuan, K. Y.-L. Yip, P.-C. Sham, P. K.-H. Tam, M.-M. Garcia-Barcelo, E. S.-W. Ngan, Identification of GENES ASSOCIATED With Hirschsprung disease, based on whole-genome sequence analysis, and potential effects on enteric nervous system development. *Gastroenterology* **155**, 1908–1922.e5 (2018).

Acknowledgments: Confocal imaging and RNA-seq were performed using equipment maintained by Li Ka Shing Faculty of Medicine Faculty Core Facility and Center for Genomic Sciences, the University of Hong Kong, respectively. **Funding:** This work was supported by research grants from the Research Grants Council (HKU17112416 and 17109215), Department of Health (HMRF 08192786 and 03143236), of Hong Kong Special Region, China, Hong Kong and a seed grant for basic research from the University of Hong Kong to E.S.-W.N. **Author contributions:** F.P.-L.L. and T.Z. conducted in vivo experiments, acquired data, and analyzed data. T.Z., A.O.W.L., S.-T.L., and W.Y.-M.W. performed in vitro assays. K.N.-C.L. and F.P.-L.L. performed the hPSC studies. Z.L. and P.-C.S. performed and supervised the bioinformatics analyses, respectively. E.S.-W.N. and C.-C.H. supervised the project and prepared the manuscript. **Competing interests:** The authors declare that they have no competing interests. **Data and materials availability:** All data needed to evaluate the conclusions in the paper are present in the paper and/or the Supplementary Materials. Raw and processed sequencing data are available in the Sequence Read Archive (SRA) at the NCBI Center with the accession number PRJNA752243 and at https://ncbi.nlm.nih.gov/bioproject/PRJNA752243. All annotated codes showing key steps of the analysis are available at https://doi.org/10.5281/zenodo.5266320. The *Kif7*$^{f/f}$ and *Gli2*$^{f/f}$ mouse lines can be provided by C.-C.H., SickKids Hospital, pending scientific review and a completed material transfer agreement. Requests for the *Kif7*$^{f/f}$ and *Gli2*$^{f/f}$ mouse lines should be submitted to C.-C.H.

Submitted 18 November 2020
Accepted 17 August 2021
Published 13 October 2021
10.1126/sciadv.abf7472

Citation: F. P.-L. Lai, Z. Li, T. Zhou, A. O. W. Leung, S.-T. Lau, K. N.-C. Lui, W. Y.-M. Wong, P.-C. Sham, C.-C. Hui, E. S.-W. Ngan, Ciliary protein Kif7 regulates Gli and Ezh2 for initiating the neuronal differentiation of enteric neural crest cells during development. *Sci. Adv.* **7**, eabf7472 (2021).